Made available by Hasselt University Library in https://documentserver.uhasselt.be

Structure and forcing of observed exchanges across the Greenland-Scotland Ridge

Peer-reviewed author version

BRINGEDAL, Carina; Eldevik, Tor; Skagseth, Øystein; Spall, Michael A. & Østerhus, Svein (2018) Structure and forcing of observed exchanges across the Greenland-Scotland Ridge. In: Journal of climate, 31 (24), p. 9881-9901.

DOI: 10.1175/JCLI-D-17-0889.1
Handle: http://hdl.handle.net/1942/26700

Structure and forcing of observed exchanges across the Greenland-Scotland Ridge

Carina Bringedal* and Tor Eldevik

Geophysical Institute and Bjerknes Centre for Climate Research, University of Bergen, Bergen, Norway

Øystein Skagseth

Institute of Marine Research, and Bjerknes Centre for Climate Research, Bergen, Norway

Michael A. Spall

Woods Hole Oceanographic Institution, Woods Hole, MA, USA

Svein Østerhus

Uni Research Climate, and Bjerknes Centre for Climate Research, Bergen, Norway

Corresponding author address: Carina Bringedal, Faculty of Sciences, Hasselt University, Campus Diepenbeek, Agoralaan building D, BE3590 Diepenbeek, Belgium

E-mail: carina.bringedal@uhasselt.be

ABSTRACT

The Atlantic Meridional Overturning Circulation and associated poleward heat transport are balanced by northern heat loss to the atmosphere and corresponding water mass transformation. The circulation of northwards flowing Atlantic Water in the surface and returning Overflow Water at depth is particularly manifested - and observed - at the Greenland-Scotland Ridge where the water masses are guided through narrow straits. There is however a rich variability in the exchange of water masses across the ridge on all time scales. Focusing on seasonal and interannual time scales, and particularly the gateways of the Denmark Strait and between Faroe Islands and Shetland, we specifically assess to what extent the exchanges of water masses across the Greenland-Scotland Ridge relate to wind forcing. On seasonal time scales, the variance explained of the observed exchanges can largely be related to large scale wind patterns, and a conceptual model shows how this wind forcing can manifest via a barotropic, cyclonic circulation. On interannual time scales the wind stress impact is less direct as baroclinic mechanisms gain importance and observations indicate a shift in the overflows from being more barotropicly to more baroclinically forced during the observation period. Overall, the observed Greenland-Scotland Ridge exchanges reflect a horizontal (cyclonic) circulation on seasonal time scales, while the interannual variability more represents an overturning circulation.

1. Introduction

The Atlantic Meridional Overturning Circulation (AMOC) and the related poleward ocean heat transport are prominent features of the Nordic Seas and Arctic Ocean (Furevik et al. 2007). The Greenland-Scotland Ridge (GSR), with its relative narrow and shallow straits separating the Atlantic Ocean from the Nordic Seas, is accordingly an excellent location for observing changes associated with the North Atlantic Current, being the Gulf Stream's northernmost limb (Figure 1). The water masses exchanged across the GSR are the poleward flow of warm and saline Atlantic Water (AW) and - from northern heat loss - the cold return flows of Polar Water (PW) freshened by river runoff, net precipitation and ice melt in the surface and dense Overflow Water (OW) at depth; the former being carried through the Denmark Strait (DS) by the East Greenland Current (EGC), and the latter are the main source for the North Atlantic Deep Water, flowing through the Denmark Strait and the Faroe Bank Channel (Dickson and Brown 1994; Hansen and Østerhus 2000; Eldevik and Nilsen 2013).

The circulation in the Nordic Seas, including the exchanges across GSR, are observed to vary on a broad range of time scales under the joint influences of momentum and buoyancy forcing. The circulation and exchanges have been estimated to be in quasi-stationary balance with regional buoyancy forcing on a time scale of about 30 years (Spall 2011; Eldevik and Nilsen 2013), with momentum within closed f/h-contours sustained by the mean wind stress (Nøst and Isachsen 2003). A large amount of waters recirculate within the closed f/h-contours in the Nordic Seas, affecting the dynamics in this region (Nøst and Isachsen 2003; Isachsen et al. 2003). Associated mechanisms for variability include a rapid barotropic response to wind-forcing and the (multi-)decadal influence of changing hydrography and buoyancy forcing (Zhang et al. 2004; Eldevik et al. 2009; Spall 2015; Behrens et al. 2017). Wind-forcing has been related to the North Atlantic

Oscillation (NAO), which is the prominent mode of sea level pressure variability in the North Atlantic (Furevik and Nilsen 2005). The forcing of northern AMOC, including the variable in- and outflows of the Nordic Seas across the GSR, remains unresolved and an issue of much scientific debate (Hansen and Østerhus 2000; Hátún et al. 2005).

The purpose of this study is to assess the observed variability in GSR exchanges (Figure 2), and in particular how this variability specifically can be explained by wind forcing alone, or by the joint influence of wind and buoyancy forcing on seasonal to interannual time scales. Our assessment is guided by the following overall questions:

- To what extent do observed variable exchanges at GSR reflect a cyclonic (horizontal) or an overturning circulation in the Nordic Seas?

- To what extent can observed volume transports at GSR be explained by the direct influence of variable winds or associated changes in sea level pressure?

- At what time scales must buoyancy effects (wind-induced, or other) be accounted for?

We emphasize that the current meter-based time series synthesized and discussed herein are the result of extensive efforts over many years by individual colleagues and institutions, and we have benefitted from these observations made publicly available by the NACLIM consortium (naclim.eu). Key publications include Berx et al. (2013); Jónsson and Valdimarsson (2005, 2012); Hansen and Østerhus (2007); Hansen et al. (2015a,b, 2016); Jochumsen et al. (2012, 2017). An earlier assessment of Atlantic exchanges concerning heat, salt and volume fluxes between the North Atlantic and the Arctic Mediterranean is available through Østerhus et al. (2005); a synthesis and update of the available observations is provided by Østerhus et al. (2018). The latter synthesis is also the basis of the data considered here.

However, observations of exchanges are not complete. While the bulk of overflow, through the Denmark Strait and Faroe Bank Channel (FBC), is relatively well observed, observations of other overflow branches are limited. The EGC is not monitored by moorings near the GSR. Atlantic Water crossing the Iceland-Faroe Ridge (IFR) continues eastward and is monitored in the Faroe Current (FC) north of the Faroe Islands. As will become evident when the available data are assessed, observed FC inflow is seemingly unrelated to other observed transports on seasonal and interannual time scales. FC inflow as presently observed can thus not be part of a literally coherent description of the exchanges across GSR. FC inflow is therefore only to a limited extent explicitly part of our presentation and inference below.

The data and methods of our study are presented in Section 2, and Section 3 characterizes the observed variability of in- and overflows, and the degree of co-variability between them. The variable exchanges are related to possible forcing on seasonal to interannual time scales in Section 4. The results are discussed in Section 5, partly guided by the conceptual model of Straneo (2006), followed by the concluding remarks of Section 6.

2. Data, methods and concepts

We give here an overview of the observations and reanalysis data utilized in this study, and methods used to characterize (co)variability in these data. Further we describe the conceptual model applied in Section 5.

a. Data

The observed exchanges across the Greenland-Scotland Ridge as referred to in Figure 1 and shown in Figure 2, are accessed through the NACLIM consortium. AW inflow through Faroe-Shetland Channel (FSC) is reported upon by Berx et al. (2013), while DS inflow is described

by Jónsson and Valdimarsson (2012). Observed AW transport in FC is documented by Hansen et al. (2015a). The OW transport through FBC is detailed by Hansen et al. (2015b, 2016), while the DS overflow is presented by Jochumsen et al. (2017). Recent observations and estimates of the overflow across the Iceland-Faroe Ridge (IFR) suggest a mean overflow of less than 0.4 Sv (Hansen et al. 2018). Observations of overflow across the Wyville-Thomson Ridge (WTR) are available, with some gaps, for 2003-2013 and are on average 0.8 Sv (Sherwin et al. 2008a; Sherwin 2010). However, due to low data coverage, IFR overflow and WTR overflow will not be considered in this study. We refer to the above publications regarding uncertainties in the observed estimates of volume transports. For all volume transports, we assess monthly averaged data.

Hydrography from the KG6 station on the Kögur section is also available through the NACLIM consortium. The Kögur section is located north of where DS overflow is measured (see Figure 1), and is reported upon in Jónsson and Valdimarsson (2012). The KG6 station measures temperature and salinity at various depths 3-4 times a year.

Gridded hydrography of the Nordic Seas extending across the GSR is available through the Nordic Sea Atlas (Korablev et al. 2014). The dataset utilizes over 500 000 stations to create temperature, salinity and density fields on a $0.25^\circ \times 0.25^\circ$ degree grid spanning 58°-84°N, 47°W-72°E at 29 depth levels for the period 1900-2012. After 1993, a total of 102 758 stations throughout the Nordic Seas are utilized. There are fewer observations near the northern coast of Greenland and north of Iceland, but sampling frequency and density is larger near the GSR, and particularly in western DS. Altimetry measured sea surface height (SSH) has been accessed through EU Copernicus Marine Service Information (CMSES) on a $0.25^\circ \times 0.25^\circ$ degree grid. From the ERA-Interim reanalysis (Dee et al. 2011) we apply surface winds, atmospheric sea level pressure (SLP) and atmospheric heat flux on a $1^\circ \times 1^\circ$ degree grid. The ERA-Interim reanalysis is considered realis-

tic for the Arctic region and the variables considered here (Lindsay et al. 2014). All the gridded datasets are monthly averages.

b. Methods

For each time series, the mean (linear trend) is subtracted and these *monthly* data are used when analyzing seasonal variability. To investigate interannual variability, we form *annual* data by applying a simple, if approximate, 12-month low-pass filter (in the form of a 25-month triangular window) to the monthly data; the annual time series are accordingly truncated by 6 months at the endpoints. Missing data points within the time series are replaced with the mean value corresponding to that month, but these data points are removed after filtering. Note that the annual data still contains 12 data points per year, but without any variability on shorter than annual time scales. For gridded datasets, the above steps are implemented for each grid point.

Covariability between two time series is determined using linear correlations based on Pearson correlation coefficient; i.e., r-values (Thomson and Emery 2014). All reported correlations are significant at a 95% (90%) confidence level based on Student's t-test for seasonal (interannual) variability (Thomson and Emery 2014), where autocorrelation is taken into account by adjusting the effective number of degrees of freedom (EDF) following Chelton (1983). Note that the adjustment of EDFs will be strongly affected by the amount of autocorrelation within the time series, hence the significance criterion can vary substantially. We perform EOF analysis (Björnsson and Venegas 1997) to resolve spatio-temporal variability in the gridded data sets. Power spectra are computed by applying the maximum entropy method (Ghil et al. 2002), and for significance testing these estimates are compared to red noise spectra computed by fitting a first order autoregressive process to the data sets.

We employ a measure of the NAO as the leading order EOF mode of annual SLP from the region 20°-90°N, 90°W-40°E. Although the NAO is usually winter-based, the leading EOF mode of the full-year SLP provides the same spatial pattern usually associated with the NAO. Derivatives of gridded data (e.g., of wind stress) are calculated through 2-point difference approach using two neighbouring grid cells. Wind stress (τ_x, τ_y) is estimated from wind data (u_x, u_y) using $(\tau_x, \tau_y) = c_D \rho_{\text{air}} \sqrt{u_x^2 + u_y^2}(u_x, u_y)$, where $c_D = 1.5 \times 10^{-3}$ and ρ_{air} is a shifted sinusoidal with maximum 1.3 kg m^{-3} in January and minimum 1.2 kg m^{-3} in July. We define the mixed layer depth (MLD) as the depth were the density has increased 0.125 kg m^{-3} compared to the density at surface, in accordance with the sigma-t criterion by Levitus (1983). When falling between two vertical grid points, linear interpolation is used.

c. Two-layer model

We adopt a modified version of the time dependent two-layer model formulated by Straneo (2006). The model contains an interior reservoir surrounded by a narrow boundary current, with parametrized eddies to communicate heat between the interior and boundary current, see Figure 3. The model has been adapted to include a sill, see discussion below. Straneo included atmospheric heat loss only from the interior reservoir and for completeness we include heat loss also from the boundary current. The two layers have fixed temperatures, with the deeper being colder than the upper. The depth of the interfaces between the two layers in the interior and the boundary current will adapt due to heat loss to the atmosphere and the eddy heat exchange, as baroclinic eddies are only active when there is a difference in the interface heights between the interior and boundary current. The boundary current velocity is only in the along-current direction and the baroclinic component is calculated from the horizontal density gradient using the thermal wind balance. The velocity is formulated as vertical averages for each layer. As the interface height in

the boundary current can vary along the current, the boundary current speed varies accordingly to preserve mass balance. For all details concerning the model derivation and assumptions we refer to Straneo (2006).

Model parameters concerning size of domains etc., are chosen in accordance with the Nordic Seas and are given in Table 1 along with the adapted model equations. The model is forced with the atmospheric heat loss from boundary current and interior, $Q_{\mathrm{bc}}(t)$ and $Q_{\mathrm{int}}(t)$, along with a barotropic component of the boundary current, see discussion below. The model is solved for the thickness of the deep layers in the interior and boundary current.

Straneo formulated her model for the Labrador Sea, which does not have a sill. Iovino et al. (2008) showed that the effect of a sill is mainly the difference in boundary current strength as the sill limits the flow that prefers to follow f/h-contours. Spall has in several papers used a similar formulation for the Nordic Seas (Spall 2011; Yasuda and Spall 2015) where the boundary current is based on thermal wind balance, and found good correspondence between this formulation and idealized numerical simulations mimicking the Nordic Seas and its boundary current. The sill affects the formulation of the model by adjusting the interior interface height, $d(t)$, into height above the sill height. The adjusted variable and the height of the deep boundary current layer, $h_2(t,l)$, are marked in Figure 3, where l indicates the along-current coordinate.

We will apply the adapted two-layer model to determine the relative importance of the baroclinic and barotropic forcing on seasonal time scales, where the baroclinic forcing is quantified through observed atmospheric heat loss. For the barotropic forcing we take into account how wind interacts with topography, as topography is of importance for the Nordic Seas (Nøst and Isachsen 2003; Spall 2011). Skagseth (2004) found that for monthly time scales a topographic Sverdrup relation (Niiler and Koblinsky 1985) applies; i.e., that positive wind stress curl integrated within a bottom contour is balanced by cross-isobath flow toward shallower depth and visa versa. Further, this

was reflected in the variability in the along-slope current in the southern Norwegian Sea at the Svinøy section (Skagseth et al. 2004). This indicates a transfer from cross- to along-isobath flow analogous to Walin et al. (2004), who argued that the northward buoyancy loss along-stream the Norwegian Atlantic Current causes a baroclinic flow toward shallower depth, that through mass conservation is transferred into an equivalent barotropic slope current. Based on satellite SSH data the slope current varies coherently across the Iceland-Scotland ridge in response to a NAO-like wind pattern (Skagseth et al. 2004). Hence, through an estimate of the length of the along-isobath region where the positive wind stress curl acts, the corresponding barotropic velocity component across the ridge can be calculated as a scaled topographic Sverdrup relation

$$v_{w,\mathrm{Sv}} = \frac{L_{\mathrm{along}}}{\rho_{\mathrm{ref}} L h^2 |\nabla(\frac{f}{h})|}\Big(\frac{\partial \tau_y}{\partial x} - \frac{\partial \tau_x}{\partial y}\Big), \tag{1}$$

where L_{along} is the length of the region where the wind stress curl pushes waters towards shallower depths and must be estimated through observations of wind stress curl and is discussed in Section 5a. Note that the Coriolis parameter f is considered constant, while the depth gradient must be estimated from the region where wind stress curl acts. Spall (2011) estimated how wind stress along the coast would have a significant impact on the variability across the GSR through Ekman transport and piling of waters near the coast, resulting in a barotropic transport along the coast following the wind direction. The resulting barotropic velocity is hence a scaled Ekman relation

$$v_{w,\mathrm{Ek}} = \frac{L_{\mathrm{along}}}{\rho_{\mathrm{ref}} h c_0} \tau_{\mathrm{along}}, \tag{2}$$

where τ_{along} is the wind stress component along the coastline, and L_{along} the length of the region where the along-coast wind stress pushes waters towards shallower depths and must be estimated through observations of wind stress and is discussed in Section 5a. Further, c_0 is the barotropic shelf wave speed.

Hence, we have two possible forms of the wind-forced barotropic velocity component of the boundary current, where both rely on towards-coast transport and increased SSH near the coast. The difference lies in relying either on wind stress curl or the wind stress. In the model, the velocity (1) or (2) is applied at the right inlet as sketched in Figure 3. We assume weak stratification in order to apply the barotropic relations to both layers, which is reasonable for the Nordic Seas (Oliver and Heywood 2003).

3. Observed Greenland-Scotland Ridge exchanges

In this section we quantify and characterize the observed variance of GSR exchanges (Figure 2) on seasonal to interannual time scales, and assess to what extent the branches of exchange covary.

a. Seasonal variability

The mean seasonal cycles of the branches are shown in the right panel of Figure 2. It is evident that FSC and DS inflows and the FBC overflow have a prominent seasonal cycle; there is also a seasonal cycle in the FC inflow and the DS overflow, although relatively muted in the total variance. Table 2 quantifies the correlation between the respective seasonal cycles and the full monthly time series, and between the seasonal cycle and a perfect sinusoid.

The seasonal cycles (Figure 2; right panel) display an anti-phase relation between FSC inflow, with FBC overflow and DS inflow; the latter are relatively weak when the former is strong (and vice verse), e.g., both FSC inflow and FBC overflow are anomalously northwards in winter. The seasonal phase of FC inflow is more northwards in winter. The less pronounced seasonal cycle of DS overflow is out of phase with DS inflow, i.e., similarly to the eastern gateway. The DS flows are qualitatively in seasonal phase over the water column and they are both anomalously southwards in winter. Hence, these five seasonal cycles broadly describe a seasonal GSR exchange of anomalous

net eastern inflow reflected in anomalous net western outflow during winter, consistent with a barotropic-like cyclonic circulation encompassing the Nordic Seas that is stronger in winter than summer.

The extent to which the above findings related to the seasonal cycles carries over to the full time series is documented in Table 3, with significant correlations ranging between 0.3 and 0.6; the correlation between the two overflows is essentialy zero (and insignificant). The FC inflow is seemingly unrelated to the other transports on seasonal time scales, except for some covariability with FBC overflow.

b. Interannual variability

In the following, we turn to the interannual variability of the observations (assessing the filtered time series also displayed in Figure 2). We emphasize that statistically confident inference is generally an issue at this time scale given the length of the record (e.g., Table 3), but we believe a characterization of observed interannual variance is still of relevance, particularly when related to possible forcing and previous findings in subsequent sections, and also noting that these observations have often been discussed in the context of climate change (Hansen et al. 2001; Zhang et al. 2004; Olsen et al. 2008; Hansen et al. 2016).

The power spectra of the four branches display a range of interannual variability, and all broadly exhibit variability on a 2-4 years time scale (Figure 4). From visual inspection of Figure 2, a most pronounced interannual-scale feature of the time series is that all transports except FC inflow were anomalously strong in 2002-2003, indicating a period of particularly strong overturning circulation in the Nordic Seas.

In general the two overflows covary (cf. Table 3), but from Figure 2 it is evident that the in-phase variation is restricted to the years following the abovementioned ”event” of strong overturning.

Restricting to 2004-2015, the two overflows share a (significant) correlation of $r = 0.82$. The (relatively few) years of the record prior to this are characterized by the overflows appearing out of phase. Furthermore, strong overflow generally follows strong FSC inflow with a 1-2 year time lag (Table 3). The FC inflow is again unrelated to the other transports, with a possible exception of DS inflow.

4. Forcing of Greenland-Scotland Ridge exchanges

In this section, we assess to what extent the observed variability on seasonal to interannual time scales of the North Atlantic - Nordic Seas exchanges (Figure 2) can be related to local or remote surface forcing, and in particular can be reflected in the spatial fields of sea level pressure, wind stress, and sea surface height. As FC inflow shows different behavior from the other currents, we will in the following focus on common forcing mechanisms for FSC inflow, FBC overflow, DS inflow and DS overflow only, and these four transports are generally implied when referring to "GSR exchanges" below.

a. Seasonal variability

The seasonal cycles of the GSR exchanges (Figure 2, right panel) are in line with a cyclonic Nordic Seas circulation including GSR exchanges that is stronger in winter than summer. This resonates with the seasonal cycle of Nordic Seas SLP, a regional-scale low that is most pronounced in winter (Furevik and Nilsen 2005). Correlation maps between the four transports (Figure 2, left panel) and reanalyzed SLP using monthly data resemble NAO-like patterns (Figure 5), with a center of action in the vicinity of Iceland and its anti-phase counterpart, normally centered off the Iberian Peninsula, being generally shifted east and partly less pronounced. The positive/negative

correlations in Figure 5 support how a lowered SLP near Iceland relates to stronger cyclonic circulation through the Nordic Seas.

The large scale SLP patterns drawn up in Figure 5 are through geostrophy associated with a positive/negative wind stress curl around the SLP center of action. Variability in wind stress curl over ocean basins are associated with cyclonic circulation anomalies through (topographic) Sverdrup balance (Eden and Willebrand 2001). The correlation maps between the transports and wind stress curl in Figure 6 show significant positive (negative) correlations near the ridge and in the Nordic Seas that are associated with cyclonic (anticyclonic) circulation anomalies of the four transports. Skagseth (2004) found that a topographic Sverdrup relation could explain monthly variability in the FSC inflow through SSH gradients both normal to and along the flow, associating SSH increases near Scotland with increased northwards flow. The correlation maps in Figure 6 support such a connection for all four transports. Note that correlations for the DS inflow and DS overflow are low, although significant.

Considering wind stress along the coast directly (Figure 7) shows how winds along the respective coastlines are associated with anomalous flow in the same direction as the wind for both inflows and overflows. We have used the southwesterly component of the wind stress as an estimate for the along-coast (or along-slope) direction. For the FSC inflow, Sherwin et al. (2008b) and Chafik (2012) found that the wind driven Ekman transport and corresponding SSH increase near Shetland resulted in increased northwards flow. Figure 7 supports such a mechanism for all four transports. The correlation values for DS overflow are low (although significant); hence, there is still much variability in the DS overflow that cannot be explained by the wind stress alone.

Note that the influences of SLP, SSH and wind are not independent. A positive phase of the NAO is for example associated both with positive wind stress curl over the Nordic Seas, strengthened westerlies (Hurrell 1995), and increased SSH near Shetland leading to an anomalously strong SSH

gradient across the FSC (Chafik 2012). Accordingly, the mechanisms explained in the above are partly interconnected.

FC inflow variability is primarily associated with SSH changes north of the GSR on seasonal and interannual time scales (Hansen et al. 2010). Richter et al. (2009, 2012) found that the FC inflow variability only depends on local wind forcing and on sea level pressure when these have a direct influence on the Nordic Seas SSH. Creating correlation maps between FC inflow and atmospheric indicators as in Figures 5-7, reveals qualitatively different patterns than for the four other currents; FC inflow is positively correlated with wind stress curl only within the Nordic Seas and with westerly wind stress at the ridge (not shown).

b. Interannual variability

There is a tendency for the mechanisms identified for the seasonal variability to translate to the interannual time scales, but admittedly much less pronounced. The annual anomalies of FSC inflow and FBC overflow in particular remain significantly correlated to an NAO-like SLP pattern and wind stress curl near the ridge, similar to Figures 5 and 6, with significant correlations peaking at $r = -0.58$ ($r = 0.47$) and $r = 0.56$ ($r = -0.72$) for FSC inflow (FBC overflow) and SLP and wind stress curl, respectively. The FSC inflow is also significantly correlated to the EOF-based NAO, with $r = 0.43$. Despite the relative shortness of the time series, there are 4 (5) positive (negative) phases of the NAO (here defined as exceeding 1 standard deviation from the mean) within the observation period.

We find, using annual data, that a positive wind stress curl anomaly averaged over the green box in Figure 1 precedes a decreased FBC overflow with 0-6 months, and a decreased DS overflow with 10-14 months (not shown). These findings are robust with respect to reasonable choices of averaging region for the wind stress curl, but correlation values are generally larger near the ridge.

A positive wind stress curl over the Nordic Seas has earlier been linked to lagged decrease in FBC and DS overflows (Yang and Pratt 2013). Using idealized simulations, Yang and Pratt (2013) found that a positive wind stress curl caused doming of the overflow reservoir through pulling the overflow waters towards the center of the basin and away from the boundary current, ultimately decreasing the overflows.

Using the annual SSH averaged over the green box in Figure 1, we find that SSH covaries with DS inflow, FSC inflow and FBC overflow transports (Table 4). Large scale SSH variability can be linked to wind-driven barotropic processes through gyre variability (Häkkinen 2001; Chafik 2012; Zhang et al. 2016), or to steric effects reflecting the heat/salt content variability (Mork and Skagseth 2005). The sign of the significant correlations supports an increased cyclonic gyre manifested through lowered SSH. Regressing the SSH gradient between the boundary current and the green box with the observations, underestimates the response following geostrophic balance with a factor 3-10 depending on which boundary current points are chosen. As the boundary current also contains waters recirculating within the Nordic Seas, it is reasonable that the geostrophic balance of the along-boundary current involves larger transport variability than what is observed across the ridge. The DS inflow, FSC inflow and FBC overflow are also correlated with the corresponding SSH differences as the boundary current SSH changes are small (not shown).

Olsen et al. (2008) found that the sum of barotropic and baroclinic pressure differences across the GSR could account for modeled FBC overflow variability on interannual time scales. Although Olsen et al. (2008) only considered the FBC overflow, the AW inflow in the southern Norwegian Sea has also been linked to along-current sea level slope on monthly to yearly time scales (Skagseth 2004). To resolve the effect of pressure differences between the Nordic Seas and North Atlantic basin on the observed exchange variability, proxies for the barotropic forces using SSH and baroclinic forcing using hydrography are constructed following Olsen et al. (2008), using the

orange boxes in Figure 1. We find that increased north-south barotropic and total pressure difference are associated with a stronger FBC overflow and weaker FSC inflow on interannual time scales, as seen in Table 5. While Olsen et al. (2008) found that the total pressure difference was necessary for the modeled FBC overflow ($r = 0.90$), our analysis using observed FBC overflow indicates that the barotropic and total pressure difference are both influential, and that this applies also to the FSC inflow.

DS overflow variability has been linked to hydraulic control through upstream interface height and SSH (Köhl et al. 2007). However, using SSH and hydrography from the Kögur section north of DS, we find neither any apparent connection between changes in DS overflow transport and the SSH variability, nor with the depth of the density interface defining the DS overflow. Also, DS inflow and overflow show no apparent connection with north-south pressures differences. Rather, the DS inflow seems to be dependent on local winds: DS inflow exhibits significant covariability with winds from south located west of Iceland, and with SSH along the western coast of Iceland, as seen in Figure 8. Hence, southern winds causing Ekman transport and consequently increased SSH near Iceland appear important for DS inflow on interannual time scales.

5. Discussion

Based on the observed variability of the four volume transports, we discuss some questions regarding forcing mechanisms. For the seasonal cycle we investigate the robustness of the wind stress or wind stress curl forcing through a two-layer model; and, focusing on the interannual variability we examine the behavior of FBC and DS overflow in particular. Finally, we discuss how the GSR exchanges can be interpreted as horizontal and overturning circulations in the Nordic Seas.

a. A simplified model describing the seasonal cycle

We apply the two-layer model presented in Section 2c, forced with average seasonal cycles of reanalyzed wind stress curl or wind stress, and atmospheric heat loss for boundary current and interior. The wind stress curl and wind stress values are the averages over where the largest significant correlations ($r > 0.4$) were found for FSC inflow (between 45°-60°N, 25°-5°W) in Figures 6 and 7. From the correlation maps we estimate L_{along} to be 1500 km for wind stress curl in (1) and 3000 km for wind stress in (2). The topographic beta $\beta = h|\nabla(f/h)|$ ranges over several magnitudes ($10^{-8} - 10^{-13}$ m^{-1} s^{-1}) in the relevant region due to variability in topography. As an estimate of the large-scale average we employ $\beta = 10^{-10}$ m^{-1} s^{-1} in (1), which is close to the arithmetic average. This value of β corresponds to a constant value of $f = 1.4 \times 10^{-4}$ s^{-1} and an average slope of about 0.5 m per km near the idealized sill. In (2), the barotropic shelf wave speed is taken as $c_0 = 10$ m s^{-1} based on the estimate by Spall (2011). The boundary current and interior heat fluxes are averages over the oceanic part of $60° - 80°$N, 25°W$-$15°E. As the observed heat fluxes are generally larger where the AW flows northwards, the model heat fluxes are weighted such that boundary current is twice as large as the interior heat flux, but the model is not sensitive with respect to this weighting. The time series of the applied forcings are seen in Figure 9. The boundary current is discretized with $\Delta l = 7500$m, while we apply a time step of 7500s to fulfill a CFL-condition. For each time step, small noise of mean 0 are added to the forcings. The model is integrated in time 15 years, and the model variables $d(t)$ and $h_2(t,l)$ reach steady seasonal cycles after 7-8 years of integration. The seasonal cycles of the inflows/outflows presented in Figure 10 are the average seasonal cycles for years 10-15. The model is compared with FSC inflow, DS inflow, FBC overflow and DS overflow, and the inflows/outflows from the two-layer model are assigned same names and sign convection as in Figure 1. The two wind forcings (1) and (2)

both rely on the presence of a longer coastline to explain the dynamics, which is not the case for FC (Richter et al. 2012). Consequently the different dynamics of FC inflow, as pointed out in in Section 4a, are not likely to be captured by this two-layer model. We will hence not attempt to include FC inflow in the following analysis.

Forcing the model with either constant or seasonally varying forcing (Figure 10) reveals that the two-layer model can largely (except for DS overflow - see discussion below) reproduce the observed seasonal cycles (Figure 2; right panel) both with respect to phase and amplitude if allowing varying wind forcing; hence, the seasonal variability of the wind is both necessary and sufficient for the GSR exchange variability. However, we cannot easily conclude whether the main driver is wind stress curl through topographic Sverdrup balance (1) or wind stress through Ekman transport (2), or both. For both the wind stress curl and wind stress forcing, there is uncertainty in determining effective parameters used in equations (1) and (2), but both equations can largely reproduce the observed seasonal cycles within reasonable choices of these parameters by themselves. Both mechanisms rely on transport towards the coast being translated into a barotropic transport through SSH stacking near the coast. Also, as both topographic Sverdrup and Ekman transport can be at play simultaneously (one below and the other in the Ekman layer), their response can be considered as the sum of (1) and (2) due to the linearity of the system. Either way, the seasonal cycle can be understood as due to barotropic mechanisms, and the effect of the seasonally varying buoyancy (baroclinic) forcing is small. This is expected from the theory of Spall (2015) because the seasonal cycle is short compared to the adjustment time of the mixed layer depth to the surface heat flux.

Although the seasonal cycles of FBC overflow and DS inflow are in overall phase when forcing the two-layer model with wind, the seasonal maxima and minima are slightly shifted. Further, the two-layer model overestimates the amplitude of the DS overflow for all cases, although it resembles the observed phase. One important point of the model is that it requires the four transports

in sum to preserve mass alone, which is in general not the case for the Nordic Seas due to contributions from Fram Strait, IFR and EGC. As the polar region and Fram Strait are not represented in the model, the part of the DS overflow fed by polar origin waters from the shelfbreak or separated East Greenland Current (see e.g., Harden et al. (2016); Behrens et al. (2017)) is not expected to be captured by the two-layer model and, as these contributions have different seasonal phases (Behrens et al. 2017), would reduce the seasonal signal. However, several modeling studies that include the polar region, e.g. Köhl et al. (2007); Serra et al. (2010); Behrens et al. (2017), describe, as the two-layer model herein, a stronger seasonal cycle in DS overflow than what is observed.

Forcing the model with wind and heat loss from the same region as earlier and including interannual variability, produces inflows/outflows with interannual variabilities with positive, but generally insignificant, correlations (when wind forcing is included) with the four respective transports (not shown). The largest (significant) correlation for interannual variability is achieved for FSC inflow when forcing the model with the southwesterly wind stress alone ($r = 0.42$). As the interannual variability of the four transports was found in Section 4b to depend strongly on other mechanisms than described by the two-layer model, the model cannot be expected to describe their interannual variability well.

Simplified two-layer models were applied to Labrador Sea and FBC overturning circulations by Deshayes et al. (2009) and Hansen and Østerhus (2007), respectively, and both models could largely reproduce the observed variability through idealized barotropic and baroclinic forcing mechanisms. Deshayes et al. (2009) found that also in the Labrador Sea the wind was more important for the seasonal variability. Hansen and Østerhus (2007) found that SSH changes (through wind forcing) had a strong influence on seasonal variability of FBC overflow, but the seasonal density field variations were the more likely forcing of the FBC overflow as the SSH-influence would overestimate the seasonal amplitude of FBC overflow. This is in contrast to the findings

of the two-layer model applied here (Figure 10) where both observed phase and amplitude of FBC overflow is well represented considering barotropic dynamics, while baroclinic forcing alone underestimates the amplitude and shifts the seasonal phase.

A plausible argument against the correlation values in Section 4a is that they could be coincidental if two independent time series exhibiting strong seasonal cycles happened to covary. However, entire time series were used in the analysis, hence including variability on shorter and longer time scales. Although not all correlations were above the 95% significance criterion, they support the hypothesis of the seasonal variability being linked to NAO-related wind-forced cyclonic circulation, which has also been indicated in earlier simulation based studies; e.g., Sandø et al. (2012). Leaning on the findings from the two-layer model, which resembles the responses both in phase and in amplitudes of the GSR exchanges satisfactory - except for the DS overflow, we can connect the seasonal variability of observed GSR exchanges to wind forcing, where both wind stress and wind stress curl can account for the observed seasonal variability.

b. Interannual variability of the overflows

The supply of overflows across the ridge will in the long term be restricted by renewal of dense waters through Nordic Seas buoyancy loss. Eldevik et al. (2009) identified time scales for dense water production and export through AW temperature and salinity anomalies manifested in the OW and found that hydrographic anomalies in FSC inflow appeared 1 (2) years later in FBC (DS) overflow. These time scales were also found in the volume transport correlations in Table 3, although not significant due to the low number of effective samples.

The annual FBC and DS overflows were found in Section 3b to covary after 2004, and were possibly anti-phased before 2002 (Figure 2). We seek to better explain the shift in interannual behavior in the overflows. As the two overflows are part of a cyclonic gyre circulation but also

drain a common overflow reservoir, in-phase variability (as after 2004) between the overflows is a sign of dominating baroclinic mechanisms, while anti-phased behavior (1995-2003) indicates barotropic forcing (Serra et al. 2010). Using a numerical simulation, Serra et al. (2010) described a NAO-forced anti-phased behavior between FBC and DS overflow, and noted that the anti-phased behavior gradually faded after 1995 due to dense water redistribution in the overflow reservoir. After 1995 the in-phase baroclinic components of the overflows increased, while the anti-phase barotropic components decreased in strength due to weaker wind forcing (Serra et al. 2010).

We calculate the average mixed layer depth (MLD) across 66°-71°N, 10°W-5°E (Figure 11). Preferably we would have expanded this averaging region further west, but as the relative error in the Nordic Sea Atlas density field is some years too large, we restrict the domain to the Norwegian Sea region. Relative errors are in the present region large certain months before 2003, but acceptable for March which is when the deepest MLDs are generally found. The annual maximum in MLD marked in Figure 11 shows how the MLD has a minimum around 2003 before it strongly increases. The average of annual maximum MLD in 1995-2003 - when the overflows appear out of phase - is 470 m, while the average annual maximum MLD after 2004 is 560 m. The increase in MLD suggests that production of deep waters escalated after 2003, indicating that a relative shift of the overflow forcing from barotropic to baroclinic seems plausible. We also note that the SSH in the Nordic Seas (average over green box in Figure 1) was anomalously strong in 2003, whose role for the Iceland-Faroe Ridge has been discussed by Olsen et al. (2016). The FSC and DS inflows as well as the FBC and DS overflows were anomalously strong at the same time (Figure 2).

Both Serra et al. (2010) and Yang and Pratt (2013) formulated how the balance between barotropic and baroclinic mechanisms can be understood through deformation of isopycnal surfaces: a weak barotropic gyre relaxes the doming of the isopycnal defining the overflow reservoir, allowing overflow waters to reach the slope current and be transported across the ridge. However,

due to in periods low data reliability it has not been feasible to use the Nordic Sea Atlas for this purpose. Hence, addressing any evidence of deforming isopycnal surfaces is beyond the scope of this work.

We find that FBC overflow is covarying stronger with Nordic Seas SSH (green box in Figure 1) and north-south barotropic pressure difference (between the orange boxes in Figure 1) before 2005. The correlation value with SSH before 2005 is $r = 0.83$ (as compared to $r = 0.67$ for the entire period, see Table 4), while correlation with the barotropic pressure difference is $r = 0.77$ (as compared to $r = 0.63$ for the entire period, see Table 5). Note however that there is only 9 years of data prior to 2005, but correlations are significant when correcting for EDF. After 2005, these correlations are weaker and not significant. Hence, before 2005 the FBC overflow was more tightly linked to barotropic forcing mechanisms while the period after 2005 is suggestively dominated by baroclinic mechanisms. Olsen et al. (2008) found a remarkable covariance between observed and modeled FBC overflow accounting for 52% (85%) of the monthly (interannual) variability until 2005. As atmospherically forced ocean GCMs generally have better skill for direct (and local) barotropic variability, the connection between FBC overflow and barotropic mechanisms before 2005 can possibly explain the strong agreement between observed values and those modeled by Olsen et al. (2008).

c. Nordic Seas overturning and horizontal circulations

As the volume exchanges of warm Atlantic Waters and cold Overflow Waters across the GSR are part of the northern limb of the Atlantic Meridional Overturning Circulation, the variability of these exchanges can be associated with variability in AMOC. We have however seen that the variability in the GSR exchanges - in particular the seasonal - can be interpreted as part of a cyclonic (horizontal) exchange. Hence, we seek to quantify to which extent the GSR exchanges

that follow the rim of the Nordic Seas reflect horizontal or overturning circulation in the Nordic Seas.

We consider FSC and DS inflow, and FBC and DS overflow volume transports as a gridded dataset representing in-/outflows in the surface and at depth, in the west part and east part of the GSR. Performing an EOF analysis on standardized anomalies of this dataset will provide objective measures of the structure of these exchanges and their relative importance. The EOF analysis is performed only between May 1996 and April 2014 to avoid periods with too low data coverage. Gaps in the time series within this time frame are filled with the current's mean value. The leading order mode of the monthly data represents a cyclonic circulation with flow towards north in the east and towards south in the west part of the ridge, while the second mode depicts overturning with northwards flow at the surface and southwards flow at depth. For the annual data the first two modes reflect overturning and cyclonic circulation, respectively. The patterns of the dominant modes together with variance explained are summarized in Table 6. We interpret these four EOF modes as indicators of monthly/annual overturning/horizontal circulation within the Nordic Seas, as manifested at the GSR. Hence, for the seasonal variability the cyclonic (horizontal) exchange dominates, while the overturning circulation is most important for the interannual variability.

The two leading monthly principal components (PCs) along with seasonal cycles and power spectra are shown in Figure 12. Their seasonal cycles explain 49% and 8% of the monthly variability. The two leading annual principal components are shown as black overlay in the left part of Figure 12. A remarkable feature of the annual PC reflecting overturning is that it also indicates anomalous strong overturning around 2003.

Eden and Willebrand (2001) and Barrier et al. (2014) described how large-scale wind patterns associated with a positive NAO give a fast, barotropic response manifested as increased cyclonic circulation quantified by a simple (topographic) Sverdrup balance, while increased overturning

is expected three years later through baroclinic adjustments. We find using monthly data that increased horizontal circulation is associated with lowered SLP near Iceland, positive wind stress curl near the ridge and wind stress along the coast (Figure 13). These findings are in-line with our previous findings of how the transports on seasonal time scales can be interpreted as part of a SLP or wind stress (curl) forced barotropic, cyclonic circulation. Using annual EOFs, the two leading modes can be associated with a rapid response through SSH; the annual SSH averaged over the green box in Figure 1 share correlation values of $r = 0.67$ and $r = -0.50$ with the annual overturning and horizontal circulations, respectively. A decreased SSH can be associated with strong cyclonic circulation (cf. Table 4), while a possible relation between SSH and overturning is discussed below. We find an indication of a positive phase of the annual EOF-based NAO is followed by increased overturning 2.5-3 years later, but the correlation is not significant due to the relative shortness of the overturning time series.

Ekman transport and associated coastal convergence can be - depending on latitude - important for AMOC variability on interannual time scales (Cabanes et al. 2008). We find that annual southerly winds and increased SSH along the continental slope on the eastern side of the Nordic Seas is associated with increased overturning circulation on annual time scales, as seen in Figure 14. However, the extent of the increased SSH region can also be an indicator of steric effects affecting the overturning; i.e., that warmer or fresher than average waters in the Norwegian Sea can be associated with increased overturning.

The above EOFs are based on standardized anomalies of the four transports, hence their PCs do not reflect values in Sverdrups. Motivated by the structure of the leading modes from Table 6, we can define physical measures of the horizontal and overturning circulation using the difference

and sum of the inflows and overflows;

$$\mathrm{HC} = \frac{1}{2}\Big(\{\text{FSC inflow}\} - \{\text{FBC overflow}\} - (\{\text{DS inflow}\} - \{\text{DS overflow}\})\Big),$$

$$\mathrm{OC} = \frac{1}{2}\Big(\{\text{DS inflow}\} + \{\text{FSC inflow}\} + \{\text{DS overflow}\} + \{\text{FBC overflow}\}\Big).$$

These two indicators do not take into account any weighting between the transports as performed by the EOF analysis, but has the advantage of giving physical estimates for the horizontal and overturning circulation. The HC and OC are however closely related with the EOFs and share correlation values of $r = 0.91$ $(r = 0.93)$ and $r = 0.87$ $(r = 0.78)$ with the corresponding PCs for the monthly (annual) variability, respectively. The mean values of the HC and OC are 1.3 Sv and 4.4 Sv, respectively, showing how these GSR exchanges in the mean mainly represent an overturning transformation. Note that these estimates are based on four transports alone, and the total GSR exchange also includes EGC and inflow and overflow across the Iceland-Faroe Ridge. In particular, the EGC would give a positive contribution to the HC and negative to the OC. Including FC inflow and WTR overflow transports by adding them to FSC inflow and FBC overflow, respectively, increases the mean HC and OC to 2.9 Sv and 6.7 Sv.

6. Conclusion

We have described the observed volume transport variability of four volume transports crossing the Greenland-Scotland Ridge: The inflow of warm Atlantic Water through the Faroe-Shetland Channel and Denmark Strait, and the overflow of cold Overflow Water through the Faroe Bank Channel and Denmark Strait. By comparing these transport time series with reanalyzed sea level pressure, wind and sea surface height, we can deduce common forcing mechanisms on seasonal and interannual time scales. The AW measured north of the Faroe Islands in the Faroe Current was

not considered regarding common forcing mechanisms as the statistical analysis revealed it being unrelated to the other transports on these time scales.

Concerning the seasonal cycle, the four transports can be interpreted as being part of a cyclonic circulation encompassing the Nordic Seas driven by the wind stress or wind stress curl near the Greenland-Scotland Ridge. Supported by a simple two-layer model based on Straneo (2006), the wind stress curl through a topographic Sverdrup relation and the wind stress through an Ekman relation can both account for the observed seasonal variability of the four transports following the rim of the Nordic Seas, both with respect to seasonal phase and amplitude. Baroclinic processes through atmospheric heat loss play a minor role for the seasonal variability.

Moving into longer time scales, the Greenland-Scotland Ridge exchanges can to some extent still be interpreted as part of a barotropic, cyclonic circulation, but baroclinic mechanisms gain importance. The Faroe Bank Channel overflow and Faroe-Shetland Channel inflow relates to a barotropic and total pressure difference across the ridge, but the connection between the Faroe Bank Channel overflow and the barotropic pressure difference is less pronounced after 2004. The interannual variabilities of the Faroe Bank Channel and Denmark Strait overflows shift from being anti-phased to in-phase during the observation period, which is linked to a shift from dominant barotropic to common baroclinic forcing mechanisms. The Faroe Bank Channel overflow is influenced by wind-induced barotropic forcing on both seasonal and longer time scales, and we find that this connection was particularly strong before 2005.

Estimating the Nordic Seas overturning and horizontal circulations through these four volume transports provides insight to the extent of horizontal transport and overturning transformation occurring within the Nordic Seas, as well as their possible relations to forcing mechanisms. In the mean, the Greenland-Scotland Ridge exchanges reflect an overturning transformation. The seasonal variability is mainly a horizontal, cyclonic circulation associated with wind stress or

wind stress curl, while the interannual variability is dominated by overturning that can be linked to winds from south and increased SSH within the Nordic Seas.

In summary, and returning to the three questions posed in the introduction:

- The observed variable exchanges across the Greenland-Scotland Ridge reflect a horizontal circulation in the Nordic Seas on seasonal time scales, and to a larger extent an overturning circulation on interannual time scales.

- The barotropic-like seasonal cycle of anomalous in- and overflow following the rim of the Nordic Seas can be explained by the direct influence of wind associated with changes in sea level pressure.

- Buoyancy effects are not essential for the seasonal variability, but must be accounted for when considering interannual time scales.

Acknowledgments. This research was supported by the Research Council of Norway project NORTH (grant number 229763). Additional support for M. A. Spall was provided by National Science Foundation grant OCE-1558742, for T. Eldevik and S. Østerhus by the European Union's Horizon 2020 research and innovation program project Blue-Action (grant number 727852), and for S. Østerhus by the European Framework Programs under grant agreement n.308299 (NACLIM).

The authors would like to thank the NACLIM consortium for accessing GSR volume transport and hydrography data. The data on which this research is based belong to the NACLIM consortium, to the team led by B. Berx at Marine Scotland (FSC inflow); by B. Hansen and K. M. H. Larsen at Havstovan (FC inflow and FBC overflow); by S. Jónsson and H. Valdimarsson at Hafrannsóknastofnunin (DS inflow and Kögur hydrography); and by D. Quadfasel and K. Jochumsen at Universität Hamburg (DS overflow). These data have been collected thanks to the funding

provided by the European Union 7th framework Programme (FP7 2007-2013), under grant agreement n.308299, www.naclim.eu.

This study has been conducted using E.U. Copernicus Marine Service Information.

References

Barrier, N., C. Cassou, J. Deshayes, and A.-M. Treguier, 2014: Response of North Atlantic Ocean circulation to atmospheric weather regimes. *Journal of Physical Oceanography*, **44 (1)**, 179–201, doi:10.1175/JPO-D-12-0217.1.

Behrens, E., K. Våge, B. Harden, A. Biastoch, and C. W. Böning, 2017: Composition and variability of the Denmark Strait Overflow Water in a high-resolution numerical model hindcast simulation. *Journal of Geophysical Research: Oceans*, **122 (4)**, 2830–2846, doi:10.1002/2016JC012158.

Berx, B., B. Hansen, S. Østerhus, K. M. H. Larsen, T. Sherwin, and K. Jochumsen, 2013: Combining in situ measurements and altimetry to estimate volume, heat and salt transport variability through the Faroe-Shetland Channel. *Ocean Science*, **9 (4)**, 639–654, doi:10.5194/os-9-639-2013.

Björnsson, H., and S. A. Venegas, 1997: A manual for EOF and SVD analyses of climatic data. *CCGCR Report*, **97 (1)**, 112–134.

Cabanes, C., T. Lee, and L.-L. Fu, 2008: Mechanisms of interannual variations of the meridional overturning circulation of the North Atlantic Ocean. *Journal of Physical Oceanography*, **38 (2)**, 467–480, doi:10.1175/2007JPO3726.1.

Chafik, L., 2012: The response of the circulation in the Faroe-Shetland Channel to the North Atlantic Oscillation. *Tellus A: Dynamic Meteorology and Oceanography*, **64 (1)**, 18 423, doi: 10.3402/tellusa.v64i0.18423.

Chelton, D. B., 1983: Effects of sampling errors in statistical estimation. *Deep Sea Research Part A. Oceanographic Research Papers*, **30 (10)**, 1083–1103, doi:10.1016/0198-0149(83)90062-6.

Dee, D. P., and Coauthors, 2011: The ERA-Interim reanalysis: configuration and performance of the data assimilation system. *Quarterly Journal of the Royal Meteorological Society*, **137 (656)**, 553–597, doi:10.1002/qj.828, URL http://dx.doi.org/10.1002/qj.828.

Deshayes, J., F. Straneo, and M. A. Spall, 2009: Mechanisms of variability in a convective basin. *Journal of marine research*, **67 (3)**, 273–303, doi:10.1357/002224009789954757.

Dickson, R. R., and J. Brown, 1994: The production of North Atlantic Deep Water: sources, rates, and pathways. *Journal of Geophysical Research: Oceans*, **99 (C6)**, 12 319–12 341, doi: 10.1029/94JC00530.

Eden, C., and J. Willebrand, 2001: Mechanism of interannual to decadal variability of the North Atlantic circulation. *Journal of Climate*, **14 (10)**, 2266–2280, doi:10.1175/1520-0442(2001) 014⟨2266:MOITDV⟩2.0.CO;2.

Eldevik, T., and J. E. Ø. Nilsen, 2013: The Arctic–Atlantic thermohaline circulation. *Journal of Climate*, **26 (21)**, 8698–8705, doi:10.1175/JCLI-D-13-00305.1.

Eldevik, T., J. E. Ø. Nilsen, D. Iovino, K. A. Olsson, A. B. Sandø, and H. Drange, 2009: Observed sources and variability of Nordic seas overflow. *Nature Geoscience*, **2 (6)**, 406–410, doi:10. 1038/NGEO518.

668 Furevik, T., C. Mauritzen, and R. Ingvaldsen, 2007: The flow of Atlantic water to the Nordic Seas
669 and Arctic Ocean. *Arctic Alpine Ecosystems and People in a Changing Environment*, Springer,
670 123–146.

671 Furevik, T., and J. Nilsen, 2005: *Large-scale atmospheric circulation variability and its impacts*
672 *on the Nordic Seas ocean climate-A review*, 105–136. American Geophysical Union, doi:10.
673 1029/158GM09.

674 Ghil, M., and Coauthors, 2002: Advanced spectral methods for climatic time series. *Reviews of*
675 *geophysics*, **40 (1)**, 3–1–3–41, doi:10.1029/2000RG000092.

676 Häkkinen, S., 2001: Variability in sea surface height: A qualitative measure for the meridional
677 overturning in the North Atlantic. *Journal of Geophysical Research: Oceans*, **106 (C7)**, 13 837–
678 13 848, doi:10.1029/1999JC000155.

679 Hansen, B., H. Hátún, R. Kristiansen, S. M. Olsen, and S. Østerhus, 2010: Stability and forcing of
680 the Iceland-Faroe inflow of water, heat, and salt to the Arctic. *Ocean Science*, **6 (4)**, 1013–1026,
681 doi:10.5194/os-6-1013-2010.

682 Hansen, B., K. Larsen, H. Hátún, R. Kristiansen, E. Mortensen, and S. Østerhus, 2015a: Transport
683 of volume, heat, and salt towards the Arctic in the Faroe Current 1993-2013. *Ocean Science*,
684 **11 (5)**, 743–757, doi:10.5194/os-11-743-2015.

685 Hansen, B., K. M. H. Larsen, H. Hátún, R. Kristiansen, E. Mortensen, and S. Østerhus, 2015b:
686 Faroe Bank Channel overflow 1995-2015. Tech. Rep. 15-02, Havstovan.

687 Hansen, B., K. M. H. Larsen, H. Hátún, and S. Østerhus, 2016: A stable Faroe Bank Channel
688 overflow 1995-2015. *Ocean Science*, **12 (6)**, 1205–1220, doi:10.5194/os-12-1205-2016.

Hansen, B., K. M. H. Larsen, S. Malskær Olsen, D. Quadfasel, K. Jochumsen, and S. Østerhus, 2018: Overflow of cold water across the Iceland-Faroe Ridge through the Western Valley. *Ocean Science Discussions*, **2018**, 1–33, doi:10.5194/os-2018-40.

Hansen, B., and S. Østerhus, 2000: North Atlantic-Nordic Seas exchanges. *Progress in Oceanography*, **45 (2)**, 109–208, doi:10.1016/S0079-6611(99)00052-X.

Hansen, B., and S. Østerhus, 2007: Faroe bank channel overflow 1995–2005. *Progress in Oceanography*, **75 (4)**, 817–856, doi:10.1016/j.pocean.2007.09.004.

Hansen, B., W. R. Turrell, and S. Østerhus, 2001: Decreasing overflow from the Nordic seas into the Atlantic Ocean through the Faroe Bank channel since 1950. *Nature*, **411 (6840)**, 927–930, doi:10.1038/35082034.

Harden, B. E., and Coauthors, 2016: Upstream sources of the Denmark Strait Overflow: Observations from a high-resolution mooring array. *Deep Sea Research Part I: Oceanographic Research Papers*, **112**, 94–112, doi:10.1016/j.dsr.2016.02.007.

Hátún, H., A. B. Sandø, H. Drange, B. Hansen, and H. Valdimarsson, 2005: Influence of the Atlantic subpolar gyre on the thermohaline circulation. *Science*, **309 (5742)**, 1841–1844, doi:10.1126/science.1114777.

Hurrell, J. W., 1995: Decadal trends in the North Atlantic Oscillation: regional temperatures and precipitation. *Science-AAAS-Weekly Paper Edition*, **269 (5224)**, 676–679, doi:10.1126/science.269.5224.676.

Iovino, D., F. Straneo, and M. A. Spall, 2008: On the effect of a sill on dense water formation in a marginal sea. *Journal of Marine Research*, **66 (3)**, 325–345, doi:10.1357/002224008786176016.

Isachsen, P. E., J. LaCasce, C. Mauritzen, and S. Häkkinen, 2003: Wind-driven variability of the large-scale recirculating flow in the nordic seas and arctic ocean. *Journal of Physical Oceanography*, **33 (12)**, 2534–2550, doi:10.1175/1520-0485(2003)033⟨2534:WVOTLR⟩2.0.CO;2.

Jochumsen, K., M. Moritz, N. Nunes, D. Quadfasel, K. M. H. Larsen, B. Hansen, H. Valdimarsson, and S. Jonsson, 2017: Revised transport estimates of the Denmark Strait overflow. *Journal of Geophysical Research: Oceans*, **122 (4)**, 3434–3450, doi:10.1002/2017JC012803.

Jochumsen, K., D. Quadfasel, H. Valdimarsson, and S. Jónsson, 2012: Variability of the Denmark Strait overflow: Moored time series from 1996-2011. *Journal of Geophysical Research: Oceans*, **117 (C12)**, doi:10.1029/2012JC008244.

Jónsson, S., and H. Valdimarsson, 2005: The flow of Atlantic water to the North Icelandic Shelf and its relation to the drift of cod larvae. *ICES Journal of Marine Science: Journal du Conseil*, **62 (7)**, 1350–1359, doi:10.1016/j.icesjms.2005.05.003.

Jónsson, S., and H. Valdimarsson, 2012: Water mass transport variability to the North Icelandic shelf, 1994-2010. *ICES Journal of Marine Science: Journal du Conseil*, **69 (5)**, 809–815, doi:10.1093/icesjms/fss024.

Köhl, A., R. H. Käse, D. Stammer, and N. Serra, 2007: Causes of changes in the Denmark Strait overflow. *Journal of physical oceanography*, **37 (6)**, 1678–1696, doi:10.1175/JPO3080.1.

Korablev, A., A. Smirnov, and O. K. Baranova, 2014: Climatological atlas of the Nordic Seas and northern North Atlantic. Tech. rep., NOAA Atlas NESDIS 77. doi:10.7289/V54B2Z78.

Levitus, S., 1983: Climatological atlas of the world ocean. *Eos, Transactions American Geophysical Union*, **64 (49)**, 962–963.

Lindsay, R., M. Wensnahan, A. Schweiger, and J. Zhang, 2014: Evaluation of seven different atmospheric reanalysis products in the Arctic. *Journal of Climate*, **27 (7)**, 2588–2606, doi:10.1175/JCLI-D-13-00014.1.

Mork, K. A., and Ø. Skagseth, 2005: *Annual sea surface height variability in the Nordic Seas*, 51–64. American Geophysical Union, doi:10.1029/158GM05.

Niiler, P. P., and C. J. Koblinsky, 1985: A local time-dependent Sverdrup balance in the eastern North Pacific Ocean. *Science*, **229 (4715)**, 754–756, doi:10.1126/science.229.4715.754.

Nøst, O. A., and P. E. Isachsen, 2003: The large-scale time-mean ocean circulation in the Nordic Seas and Arctic Ocean estimated from simplified dynamics. *Journal of Marine Research*, **61 (2)**, 175–210, doi:10.1357/002224003322005069.

Oliver, K. I., and K. J. Heywood, 2003: Heat and freshwater fluxes through the Nordic Seas. *Journal of physical oceanography*, **33 (5)**, 1009–1026, doi:10.1175/1520-0485(2003)033⟨1009:HAFFTT⟩2.0.CO;2.

Olsen, S., B. Hansen, S. Østerhus, D. Quadfasel, and H. Valdimarsson, 2016: Biased thermohaline exchanges with the Arctic across the Iceland-Faroe Ridge in ocean climate models. *Ocean Science*, **12 (2)**, 545–560, doi:10.5194/os-12-545-2016.

Olsen, S. M., B. Hansen, D. Quadfasel, and S. Østerhus, 2008: Observed and modelled stability of overflow across the Greenland-Scotland ridge. *Nature*, **455 (7212)**, 519–522, doi:10.1038/nature07302.

Østerhus, S., W. R. Turrell, S. Jónsson, and B. Hansen, 2005: Measured volume, heat, and salt fluxes from the Atlantic to the Arctic Mediterranean. *Geophysical Research Letters*, **32 (7)**, doi:10.1029/2004GL022188.

Østerhus, S., and Coauthors, 2018: Arctic Mediterranean Exchanges, in preparation.

Richter, K., T. Furevik, and K. A. Orvik, 2009: Effect of wintertime low-pressure systems on the Atlantic inflow to the Nordic seas. *Journal of Geophysical Research: Oceans*, **114 (C9)**, doi:10.1029/2009JC005392.

Richter, K., O. Segtnan, and T. Furevik, 2012: Variability of the atlantic inflow to the nordic seas and its causes inferred from observations of sea surface height. *Journal of Geophysical Research: Oceans*, **117 (C4)**, doi:10.1029/2011JC007719.

Sandø, A. B., J. E. Nilsen, T. Eldevik, and M. Bentsen, 2012: Mechanisms for variable North Atlantic-Nordic seas exchanges. *Journal of Geophysical Research: Oceans*, **117 (C12)**, doi:10.1029/2012JC008177.

Serra, N., R. H. Käse, A. Köhl, D. Stammer, and D. Quadfasel, 2010: On the low-frequency phase relation between the Denmark Strait and the Faroe-Bank Channel overflows. *Tellus A*, **62 (4)**, 530–550, doi:10.1111/j.1600-0870.2010.00445.x.

Sherwin, T. J., 2010: Observations of the velocity profile of a fast and deep oceanic density current constrained in a gully. *Journal of Geophysical Research: Oceans*, **115 (C3)**, doi:10.1029/2009JC005557.

Sherwin, T. J., C. R. Griffiths, M. E. Inall, and W. R. Turrell, 2008a: Quantifying the overflow across the Wyville Thomson Ridge into the Rockall Trough. *Deep Sea Research Part I: Oceanographic Research Papers*, **55 (4)**, 396 – 404, doi:https://doi.org/10.1016/j.dsr.2007.12.006.

Sherwin, T. J., S. L. Hughes, W. R. Turrell, B. Hansen, and S. Østerhus, 2008b: Wind-driven monthly variations in transport and the flow field in the Faroe-Shetland Channel. *Polar Research*, **27 (1)**, 7–22, doi:10.1111/j.1751-8369.2007.00036.x.

776 Skagseth, Ø., 2004: Monthly to annual variability of the Norwegian Atlantic slope current: con-
777 nection between the northern North Atlantic and the Norwegian Sea. *Deep Sea Research Part*
778 *I: Oceanographic Research Papers*, **51 (3)**, 349–366, doi:10.1016/j.dsr.2003.10.014.

779 Skagseth, Ø., K. A. Orvik, and T. Furevik, 2004: Coherent variability of the Norwegian Atlantic
780 Slope Current derived from TOPEX/ERS altimeter data. *Geophysical Research Letters*, **31 (14)**,
781 doi:10.1029/2004GL020057, L14304.

782 Spall, M. A., 2011: On the role of eddies and surface forcing in the heat transport and over-
783 turning circulation in marginal seas. *Journal of Climate*, **24 (18)**, 4844–4858, doi:0.1175/
784 2011JCLI4130.1.

785 Spall, M. A., 2015: Thermally forced transients in the thermohaline circulation. *Journal of Physi-*
786 *cal Oceanography*, **45 (11)**, 2820–2835, doi:10.1175/JPO-D-15-0101.1.

787 Straneo, F., 2006: On the connection between dense water formation, overturning, and poleward
788 heat transport in a convective basin. *Journal of physical oceanography*, **36 (9)**, 1822–1840,
789 doi:10.1175/JPO2932.1.

790 Thomson, R. E., and W. J. Emery, 2014: *Data analysis methods in physical oceanography*.
791 Newnes.

792 Walin, G., G. Broström, J. Nilsson, and O. Dahl, 2004: Baroclinic boundary currents with down-
793 stream decreasing buoyancy: A study of an idealized Nordic Seas system. *Journal of Marine*
794 *Research*, **62 (4)**, 517–543, doi:10.1357/0022240041850048.

795 Yang, J., and L. J. Pratt, 2013: On the effective capacity of the dense-water reservoir for the Nordic
796 Seas overflow: some effects of topography and wind stress. *Journal of Physical Oceanography*,
797 **43 (2)**, 418–431, doi:10.1175/JPO-D-12-087.1.

798 Yasuda, Y., and M. A. Spall, 2015: Influences of time-dependent precipitation on water mass trans-
799 formation, heat fluxes, and deep convection in marginal seas. *Journal of Physical Oceanogra-*
800 *phy*, **45 (7)**, 1822–1842, doi:10.1175/JPO-D-14-0147.1.

801 Zhang, J., K. A. Kelly, and L. Thompson, 2016: The role of heating, winds, and topography on
802 sea level changes in the North Atlantic. *Journal of Geophysical Research: Oceans*, **121 (5)**,
803 2887–2900, doi:10.1002/2015JC011492.

804 Zhang, J., M. Steele, D. A. Rothrock, and R. W. Lindsay, 2004: Increasing exchanges at
805 Greenland-Scotland Ridge and their links with the North Atlantic Oscillation and Arctic sea
806 ice. *Geophysical research letters*, **31 (9)**, doi:10.1029/2003GL019304.

LIST OF TABLES

Table 1. Model equations for the two layer model formulated through the unknowns $d(t)$ and $h_2(t,l)$, along with parameter values ensuring applicability for the Nordic Seas and GSR, and other relevant notation. 39

Table 2. Seasonality of GSR inflow and overflow branches. The first column quantifies the correlation between the observed exchanges (Figure 2; left panel) and by the mean seasonal cycles (Figure 2; right panel), and the second column quantifies to what extent the seasonal cycles are perfectly sinusoidal, calculated as the maximum correlation with a shifted sinusoidal function. Insignificant correlations are in italics. 40

Table 3. Covariance of GSR exchanges. Correlations for monthly (annual) data are quantified in the upper (lower, in bold) diagonal. Monthly correlations are given at no lag, while the interannual correlations are also given for number of years lag of largest correlation (a positive lag implies that the flow defining the column is leading). Interannual correlations are generally insignificant due to a small number of EDF. The EDFs ranges from 6-10 for the annual data to over 40 regarding monthly DS overflow. 41

Table 4. Correlation values between annual volume transport time series and SSH averaged over 66°-71°N, 18°W-5°E (green box in Figure 1). Insignificant correlations are in italics. 42

Table 5. Relations between FSC inflow and FBC overflow with pressure differences. Correlation values between the annual volume transport time series and the barotropic (first column), baroclinic (second column) and total (third column) pressure difference between north and south of the current passage. For FSC inflow the pressure difference is between 64°-66°N, 0°-4°W and 58°-60°N, 7°-9°W, while for FBC overflow the average pressures are between 64°-66°N, 0°-4°W and 60°-61°N, 16°-18°W. These boxes are marked with orange in Figure 1. The baroclinic pressure differences have been calculated at 200m depth for FSC inflow, and at 700m depth for FBC overflow. Insignificant correlations are in italics. 43

Table 6. Dominant EOF modes of the four exchanges. The patterns reflect the four exchanges across the GSR as seen from south, where "x" depicts northwards flow and "o" southwards. The bottom row shows the variance explained by the mode. 44

841 TABLE 1. Model equations for the two layer model formulated through the unknowns $d(t)$ and $h_2(t,l)$, along
842 with parameter values ensuring applicability for the Nordic Seas and GSR, and other relevant notation.

Equation / parameter	Description
$\frac{\mathrm{d}}{\mathrm{d}t}d(t) = -\frac{cv^*}{Ah}\int_0^P \big(d(t)-h_2(t,l)\big)^2 dl + \frac{Q_{\mathrm{int}}}{\rho_{\mathrm{ref}}c_p\Delta T}$	Buoyancy conservation interior
$\frac{\partial}{\partial t}h_2(t,l) + v_{\mathrm{adv}}(d(t),h_2(t,l))\frac{\partial}{\partial l}h_2(t,l) =$	Buoyancy conservation
$\frac{cv^*}{Lh}\big(d(t)-h_2(t,l)\big)^2 + \frac{Q_{\mathrm{bc}}}{\rho_{\mathrm{ref}}c_p\Delta T}$	boundary current
$c = 0.066$	Eddy heat flux coefficient
$A = 1.2\times10^{12}$ m^2	Interior area
$h = 750$ m	Sill depth
$L = 80$ km	Boundary current width
$P = 4000$ km	Boundary current length
$\rho_{\mathrm{ref}} = 999.8$ kg m^{-3}	Reference density
$c_p = 3.9\times10^3$ J kg^{-1} K^{-1}	Heat capacity
$\Delta T = 4.5$ K	Temperature difference AW & OW
$f = 1.4\times10^{-4}$ s^{-1}	Coriolis parameter
$\alpha_T = 0.2$ kg m^{-3} K^{-1}	Thermal expansion
$\eta = 0.5$	Baroclinic velocity fraction at inflow
$v^* = \frac{2\alpha_T\Delta T g h}{\rho f L}$	Measure of baroclinic flow
$v_{\mathrm{adv}}(d,h_2) = v_2(d,h_2) + \frac{v^*h_2}{h^2}(d+h-2h_2)$	Advective velocity
$v_1(d,h_2) = v_{\mathrm{btp}}(d,h_2(l=0)) + \frac{h_2}{h}v_{\mathrm{bcl}}(d,h_2)$	Top layer velocity
$v_2(d,h_2) = v_{\mathrm{btp}}(d,h_2(l=0)) + \frac{h_2-h}{h}v_{\mathrm{bcl}}(d,h_2)$	Deep layer velocity
$v_{\mathrm{btp}}(d,h_2(l=0)) = v_w + v_{\mathrm{bcl}}(d,h_2(l=0))\frac{\eta-h_2(l=0)}{h}$	Barotropic velocity, v_w from (1) or (2)
$v_{\mathrm{bcl}}(d,h_2) = v^*\frac{d-h_2}{h}$	Baroclinic velocity

843 TABLE 2. Seasonality of GSR inflow and overflow branches. The first column quantifies the correlation
844 between the observed exchanges (Figure 2; left panel) and by the mean seasonal cycles (Figure 2; right panel),
845 and the second column quantifies to what extent the seasonal cycles are perfectly sinusoidal, calculated as the
846 maximum correlation with a shifted sinusoidal function. Insignificant correlations are in italics.

	Monthly time series	Sinusoid
FSC inflow	0.57	0.95
FC inflow	*0.40*	0.94
DS inflow	0.71	0.99
FBC overflow	0.61	0.92
DS overflow	*0.25*	*0.83*

TABLE 3. Covariance of GSR exchanges. Correlations for monthly (annual) data are quantified in the upper (lower, in bold) diagonal. Monthly correlations are given at no lag, while the interannual correlations are also given for number of years lag of largest correlation (a positive lag implies that the flow defining the column is leading). Interannual correlations are generally insignificant due to a small number of EDF. The EDFs ranges from 6-10 for the annual data to over 40 regarding monthly DS overflow.

	FSC inflow	FC inflow	DS inflow	FBC overflow	DS overflow
FSC inflow	1	*0.09*	-0.37	-0.42	0.37
FC inflow	***0.05@0***	1	*-0.14*	-0.36	*0.04*
DS inflow	***-0.02*@0**	***-0.47@0***	1	0.58	-0.29
FBC overflow	***-0.11*@0; *0.37*@1**	***-0.28@0***	**0.57@0**	1	*-0.05*
DS overflow	***0.38*@0; *0.35*@2**	***0.04@0***	***0.10*@0**	**0.50@0**	1

852 TABLE 4. Correlation values between annual volume transport time series and SSH averaged over 66°-71°N,
853 18°W-5°E (green box in Figure 1). Insignificant correlations are in italics.

	SSH
FSC inflow	-0.43
DS inflow	0.71
FBC overflow	0.67
DS overflow	*0.11*

TABLE 5. Relations between FSC inflow and FBC overflow with pressure differences. Correlation values between the annual volume transport time series and the barotropic (first column), baroclinic (second column) and total (third column) pressure difference between north and south of the current passage. For FSC inflow the pressure difference is between 64°-66°N, 0°-4°W and 58°-60°N, 7°-9°W, while for FBC overflow the average pressures are between 64°-66°N, 0°-4°W and 60°-61°N, 16°-18°W. These boxes are marked with orange in Figure 1. The baroclinic pressure differences have been calculated at 200m depth for FSC inflow, and at 700m depth for FBC overflow. Insignificant correlations are in italics.

	$\Delta P_{\text{barotropic}}$	$\Delta P_{\text{baroclinic}}$	$\Delta P_{\text{baroclinic}} + \Delta P_{\text{barotropic}}$
FSC inflow	-0.51	*0.12*	*-0.48*
FBC overflow	0.63	*0.45*	0.67

TABLE 6. Dominant EOF modes of the four exchanges. The patterns reflect the four exchanges across the GSR as seen from south, where ”x” depicts northwards flow and ”o” southwards. The bottom row shows the variance explained by the mode.

	EOF1 monthly	EOF2 monthly	EOF1 annual	EOF2 annual
Inflow	o x	x x	x x	o x
Overflow	o x	o o	o o	o x
Contribution	53%	24%	46%	33%

LIST OF FIGURES

Fig. 1. The exchanges across the Greenland-Scotland Ridge. Red arrows indicate AW inflow, black indicate OW; solid lines are the observed flows considered in this study. The blue (stippled) represents the EGC. The green dashed line is the Kögur section. The boxes are regions used to define possible external forcing as described in Section 4, where the green box (66°-71°N, 18°W-5°E) is used for average SSH and wind stress curl, while the orange boxes (64°-66°N, 0°-4°W; 58°-60°N, 7°-9°W, and 60°-61°N, 16°-18°W) are used for a north-south pressure difference across the ridge. Isobaths are outlined for every 500m. 47

Fig. 2. Current-meter based monthly time series of volume transports across GSR. All values are in Sv, with positive directions coinciding with arrows in Figure 1. Black lines in the left panel are low-pass filtered with a 25-month triangular filter. The right panel gives the mean seasonal cycle including the 95% confidence intervals based on Student's t-test around the overall mean (dotted). 48

Fig. 3. Two-layer model with boundary current and motionless interior based on Straneo (2006). Atlantic Water is depicted in red and Overflow Water in purple. The height of the deep layer in the boundary current, $h_2(t,l)$, and height above sill depth of the interior deep layer, $d(t)$, are marked. The two layers of the beginning and the end of the boundary current defines the two inflows and outflows across the ridge. Orange arrows indicate atmospheric heat loss; green curls indicate eddy exchange. The yellow arrows represent the wind-forced barotropic part of the boundary current. 49

Fig. 4. Power spectra of GSR exchanges. Power spectra of the monthly data (with seasonal cycle removed) together with a red noise spectrum (thin line; cf Section 2b) and 95% confidence level (thin dashed line). 50

Fig. 5. Correlations between monthly SLP with AW inflow (top) and OW (bottom). Left panels are DS, right panels FSC/FBC. Dots indicate significant correlations. Note that cross-covariance in the SLP data is larger over the Nordic Seas than over continental Scandinavia, and hence the significance criterion is larger over the ocean as the EDFs are lower (approximately 20). Also, the EDFs are generally larger for DS overflow (more than 50) giving a lower significance criterion. 51

Fig. 6. Correlations between monthly wind stress curl with AW inflow (top) and OW (bottom). Left panels are DS, right panels FSC/FBC. Dots indicate significant correlations. Note that the number of EDFs varies over a broad range (but are generally close to 20). Also, the EDFs are generally larger for DS overflow (more than 50) giving a lower significance criterion. . . 52

Fig. 7. Correlations between monthly southwesterly wind stress with AW inflow (top) and OW (bottom). Left panels are DS, right panels FSC/FBC. Dots indicate significant correlations. Note that the number of EDFs varies over a broad range (but are generally close to 20). Also, the EDFs are generally larger for DS overflow (more than 50) giving a lower significance criterion. 53

Fig. 8. Correlations between annual DS inflow and wind from south (left) and SSH (right). Dots indicate significant correlations. 54

Fig. 9. Applied forcing for the two-layer model. Seasonal cycles of atmospheric heat flux for the interior, Q_{int}, wind stress curl and wind stress. 55

Fig. 10. Seasonal cycles of the in- and outflow of the two-layer model. Resulting seasonal cycles when the model is forced with: (i) seasonally varying atmospheric heat flux and wind (left); (ii) seasonally varying wind and constant atmospheric heat flux (middle); and, (iii) seasonally varying atmospheric heat flux and constant wind (right). In the first row wind forcing is through wind stress curl using (1), while in the second row wind forcing is through wind stress using (2). The two cases applying constant wind forcing, (iii1) and (iii2), give equal results. The bottom right plot (obs) instead shows the average seasonal cycles from Figure 2. Exchanges are given same names and sign convention as in Figure 2. All curves from the two-layer model are low-pass filtered with a 1month Hanning filter. 56

Fig. 11. Norwegian Sea mixed layer depth. Monthly (red) and annual maximum (black dots) regionally averaged MLD over 66°-71°N, 10°W-5°E. 57

Fig. 12. Horizontal and overturning circulation in the Nordic Seas. Left: PCs of monthly EOFs representing horizontal (top) and overturning (bottom) in colors, with corresponding PCs of annual data as black overlay. The y-axis reflects standardized anomalies. Middle: Average seasonal cycles of the monthly PCs with 95% errorbars. Right: Power spectra of the monthly PCs (with seasonal cycle removed) together with red noise (thin line) and 95% confidence level (thin dashed line). 58

Fig. 13. Atmospheric forcing of the seasonal horizontal circulation. Correlation maps between the monthly horizontal circulation (PC1) and gridded SLP (left), wind stress curl (middle) and southwesterly wind stress (right). Dots indicate significant correlations. 59

Fig. 14. Atmospheric forcing of the annual overturning circulation. Correlation maps between the annual overturning circulation (PC1) and gridded southern winds (left) and SSH (right). Dots indicate significant correlations. 60

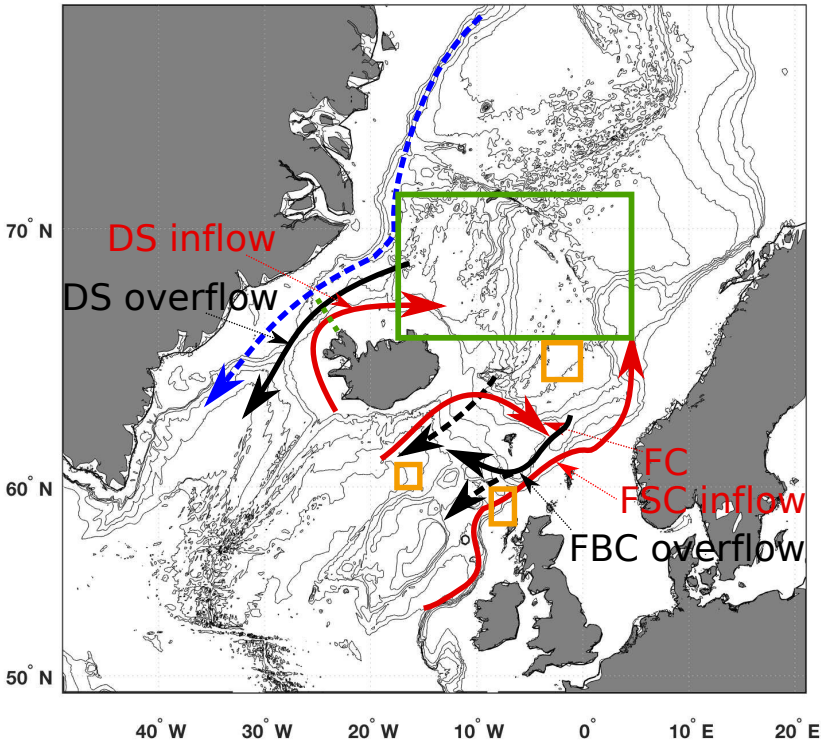

929 FIG. 1. The exchanges across the Greenland-Scotland Ridge. Red arrows indicate AW inflow, black indi-
930 cate OW; solid lines are the observed flows considered in this study. The blue (stippled) represents the EGC.
931 The green dashed line is the Kögur section. The boxes are regions used to define possible external forcing as
932 described in Section 4, where the green box (66°-71°N, 18°W-5°E) is used for average SSH and wind stress
933 curl, while the orange boxes (64°-66°N, 0°-4°W; 58°-60°N, 7°-9°W, and 60°-61°N, 16°-18°W) are used for a
934 north-south pressure difference across the ridge. Isobaths are outlined for every 500m.

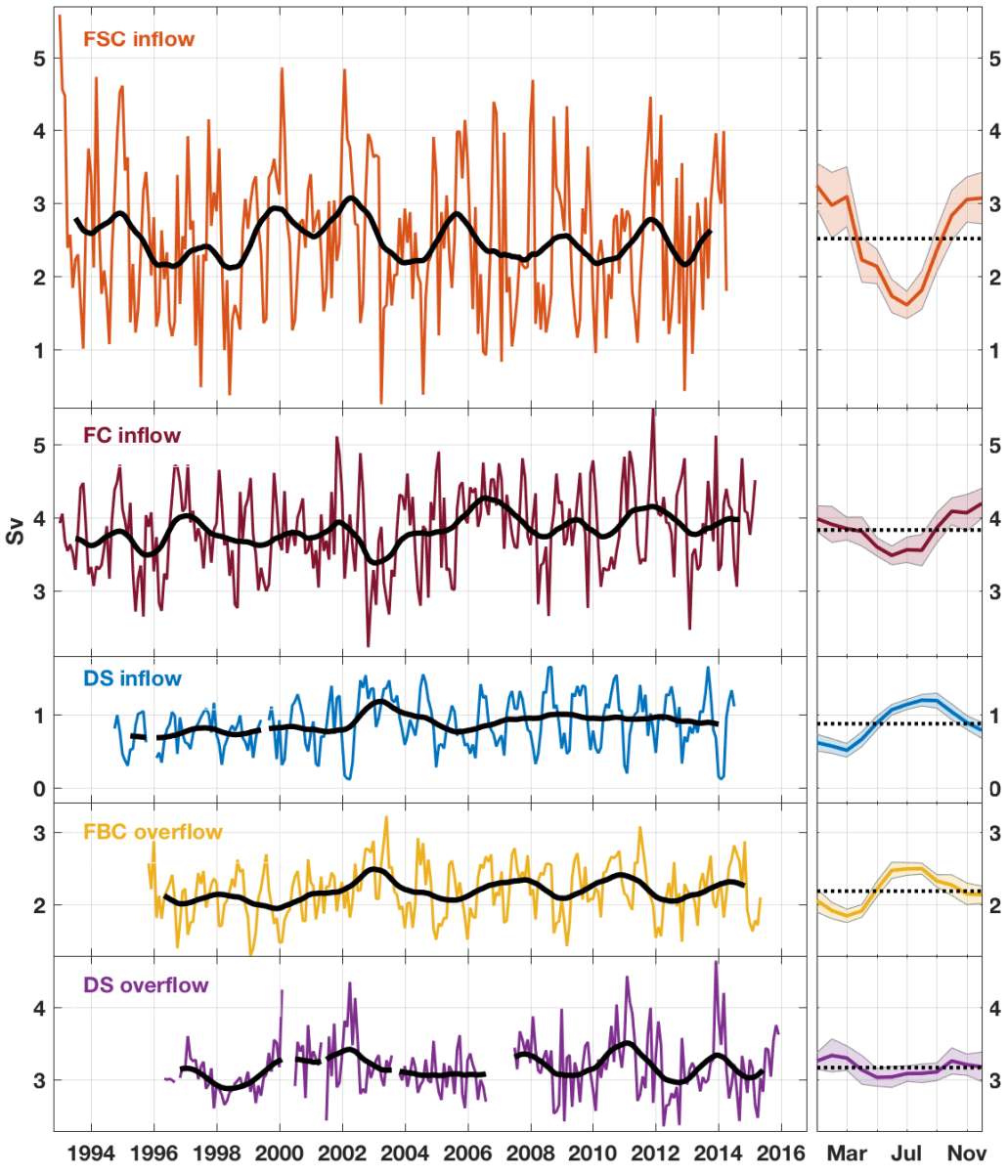

935 FIG. 2. Current-meter based monthly time series of volume transports across GSR. All values are in Sv, with
936 positive directions coinciding with arrows in Figure 1. Black lines in the left panel are low-pass filtered with a
937 25-month triangular filter. The right panel gives the mean seasonal cycle including the 95% confidence intervals
938 based on Student's t-test around the overall mean (dotted).

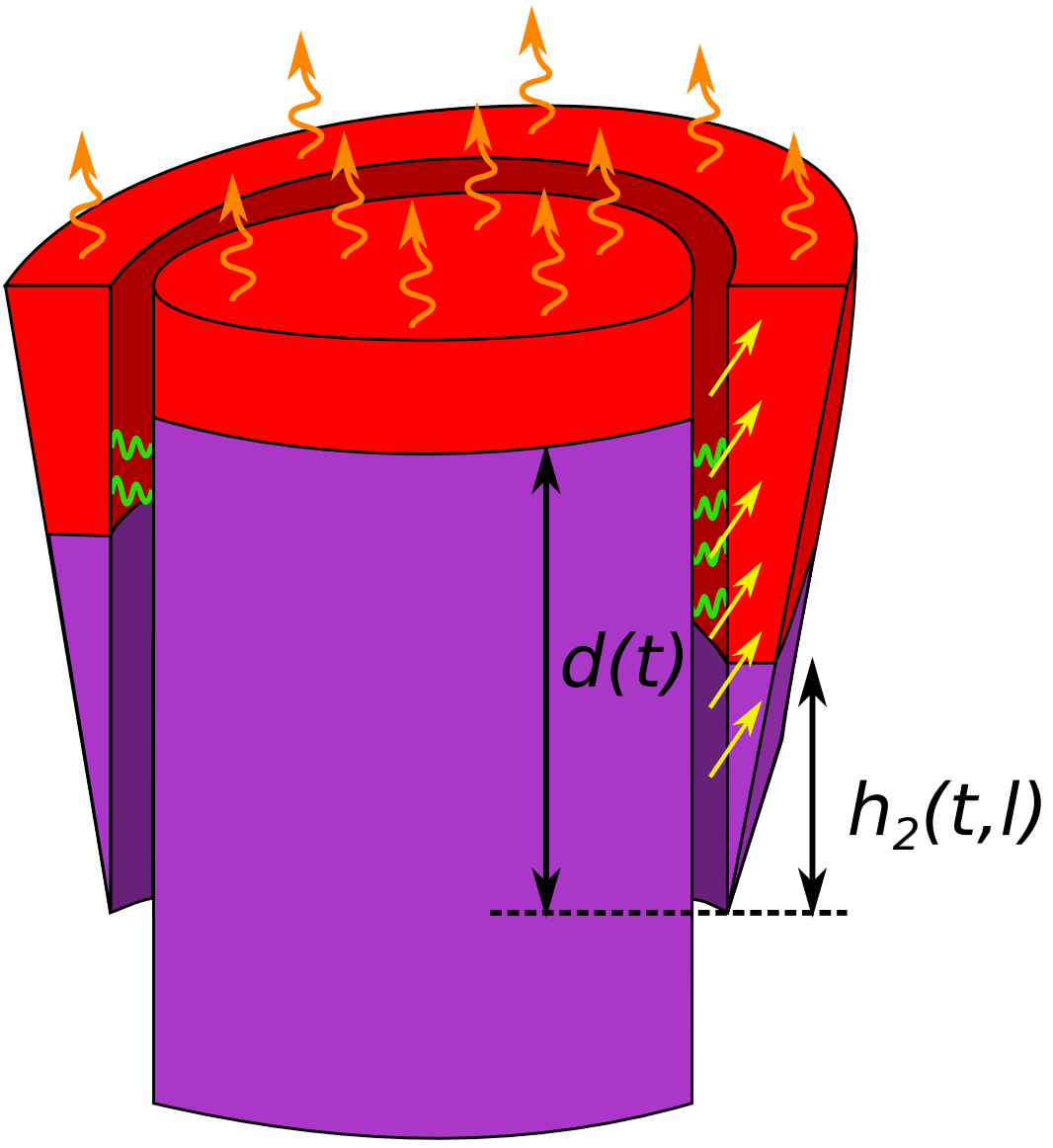

939 FIG. 3. Two-layer model with boundary current and motionless interior based on Straneo (2006). Atlantic
940 Water is depicted in red and Overflow Water in purple. The height of the deep layer in the boundary current,
941 $h_2(t,l)$, and height above sill depth of the interior deep layer, $d(t)$, are marked. The two layers of the beginning
942 and the end of the boundary current defines the two inflows and outflows across the ridge. Orange arrows
943 indicate atmospheric heat loss; green curls indicate eddy exchange. The yellow arrows represent the wind-
944 forced barotropic part of the boundary current.

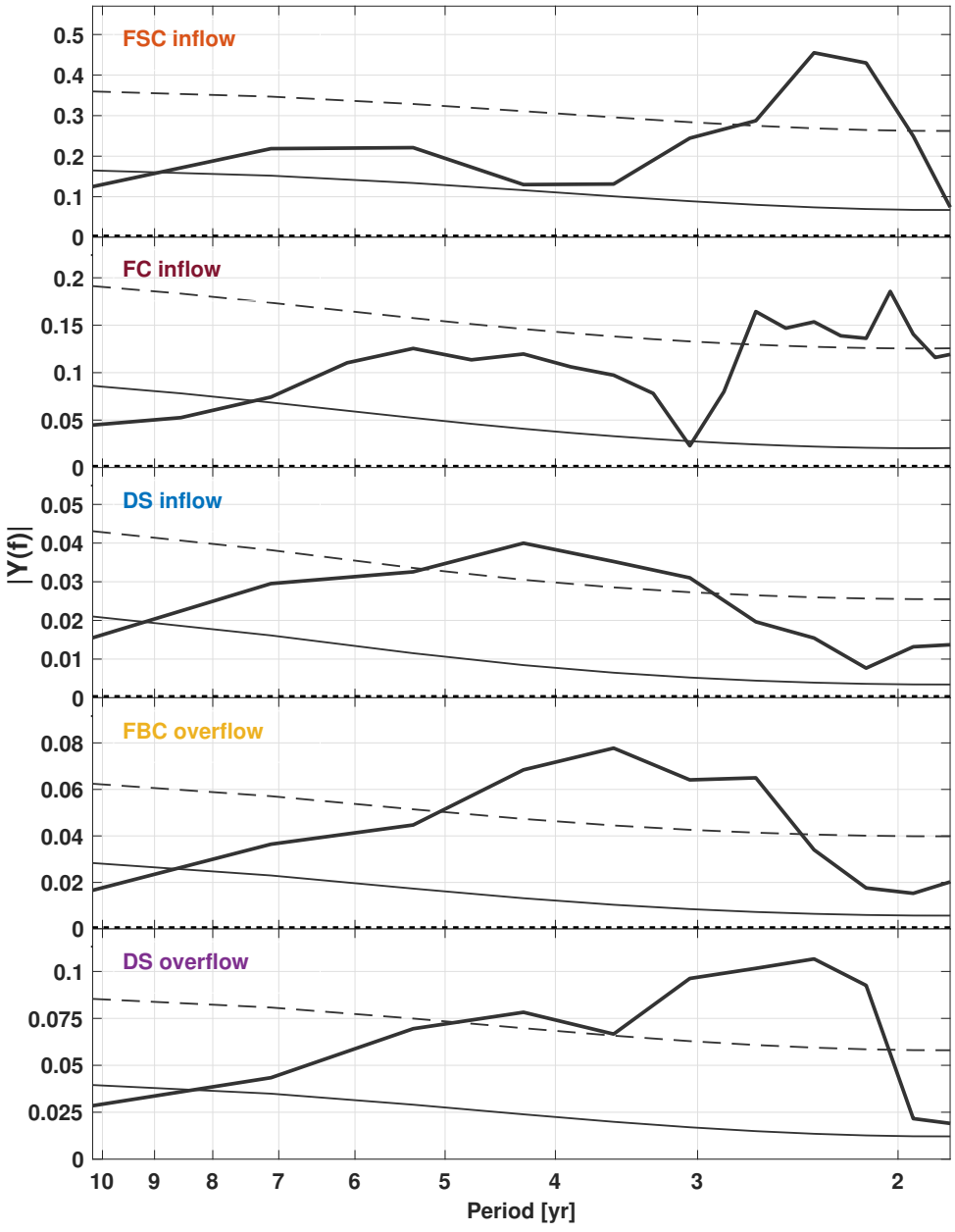

945 FIG. 4. Power spectra of GSR exchanges. Power spectra of the monthly data (with seasonal cycle removed)
946 together with a red noise spectrum (thin line; cf Section 2b) and 95% confidence level (thin dashed line).

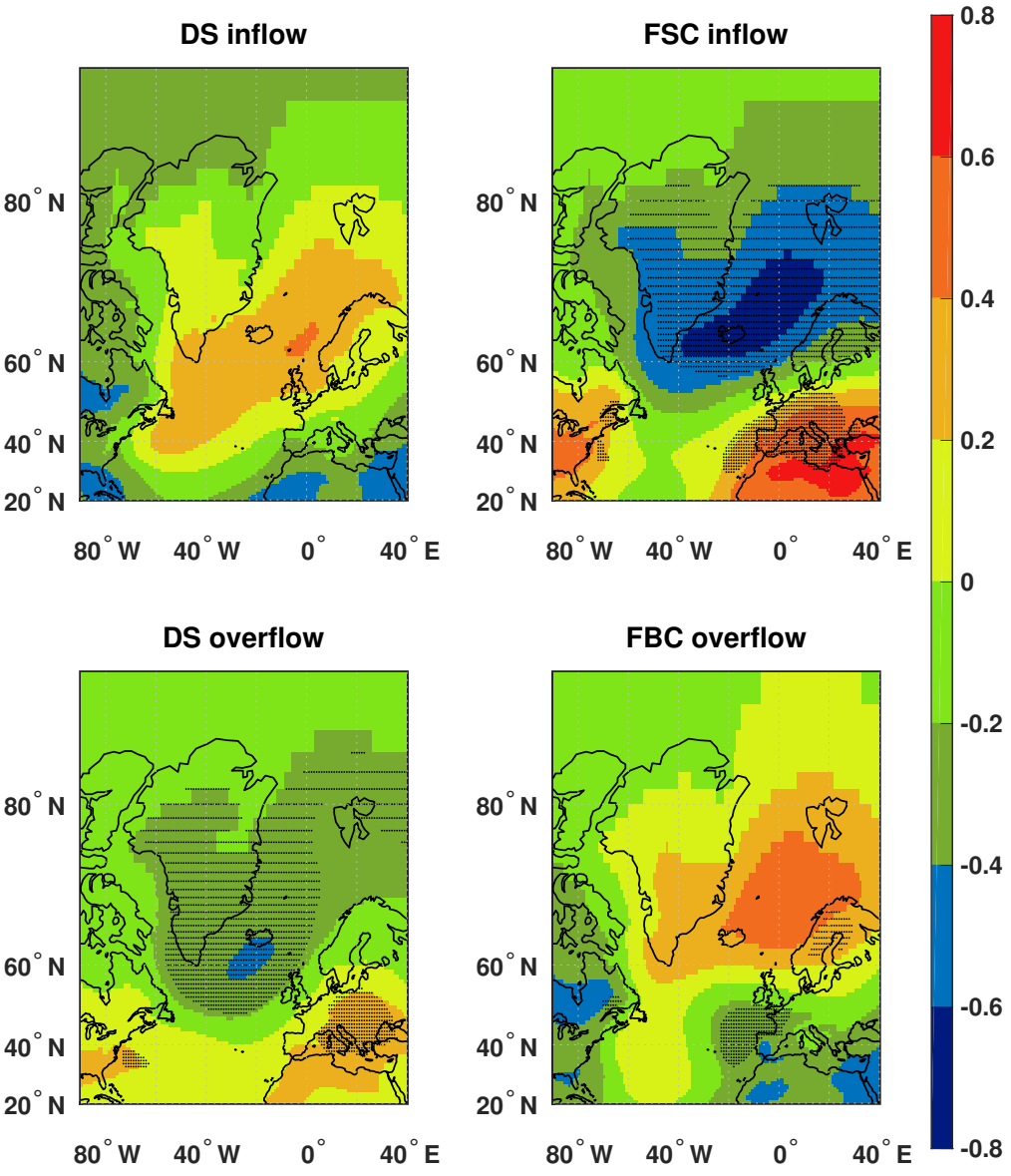

FIG. 5. Correlations between monthly SLP with AW inflow (top) and OW (bottom). Left panels are DS, right panels FSC/FBC. Dots indicate significant correlations. Note that cross-covariance in the SLP data is larger over the Nordic Seas than over continental Scandinavia, and hence the significance criterion is larger over the ocean as the EDFs are lower (approximately 20). Also, the EDFs are generally larger for DS overflow (more than 50) giving a lower significance criterion.

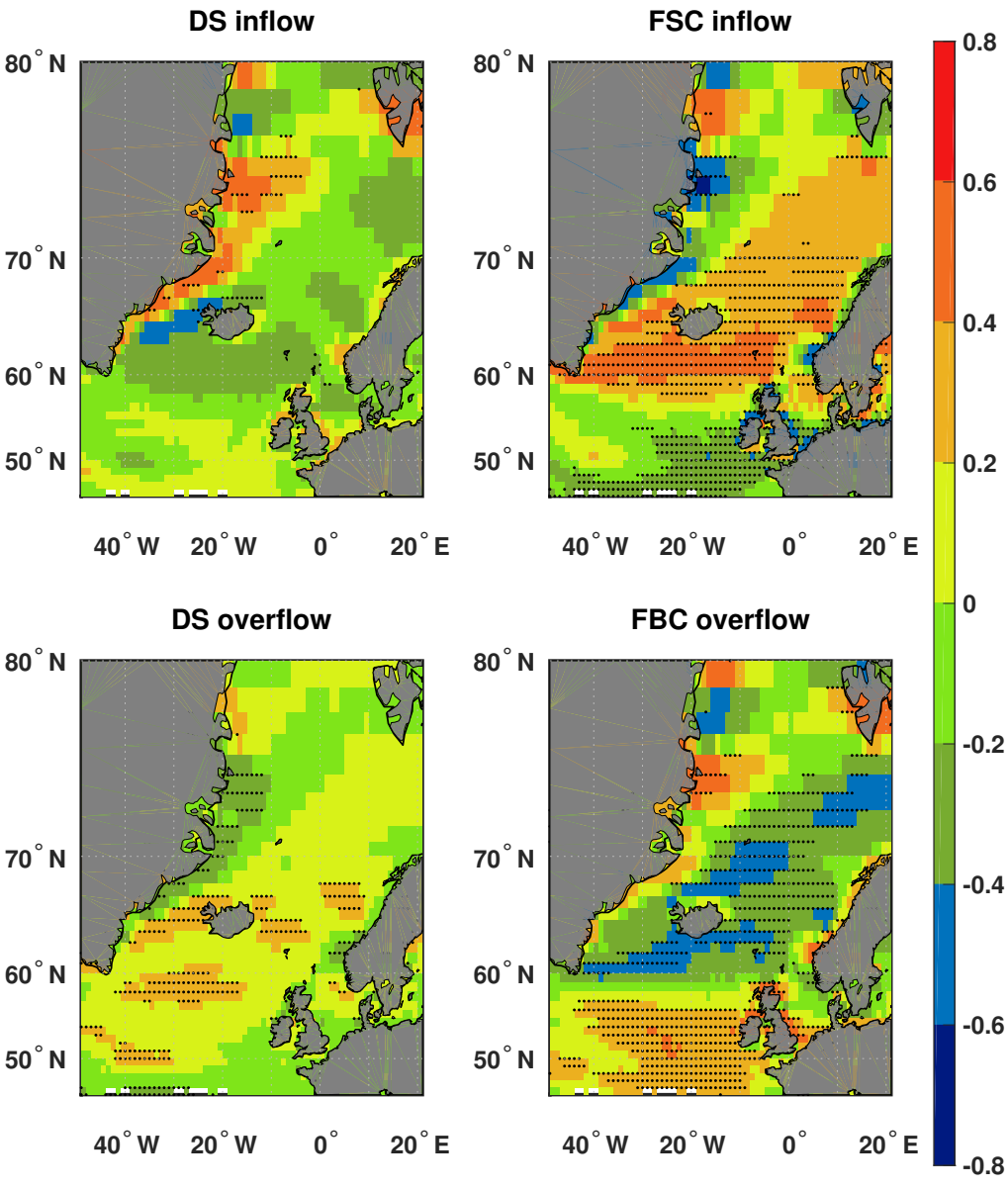

FIG. 6. Correlations between monthly wind stress curl with AW inflow (top) and OW (bottom). Left panels are DS, right panels FSC/FBC. Dots indicate significant correlations. Note that the number of EDFs varies over a broad range (but are generally close to 20). Also, the EDFs are generally larger for DS overflow (more than 50) giving a lower significance criterion.

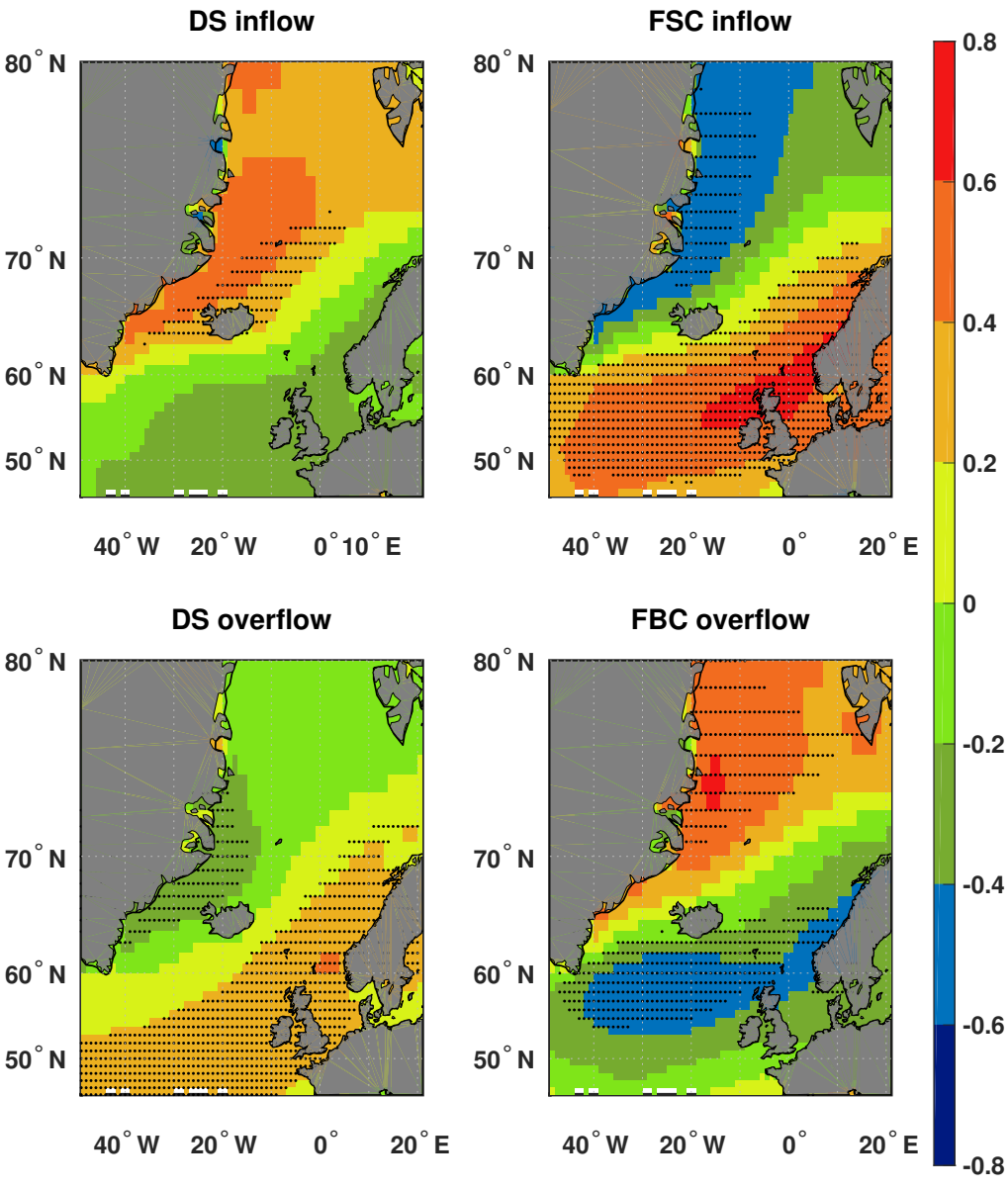

956 FIG. 7. Correlations between monthly southwesterly wind stress with AW inflow (top) and OW (bottom).
957 Left panels are DS, right panels FSC/FBC. Dots indicate significant correlations. Note that the number of EDFs
958 varies over a broad range (but are generally close to 20). Also, the EDFs are generally larger for DS overflow
959 (more than 50) giving a lower significance criterion.

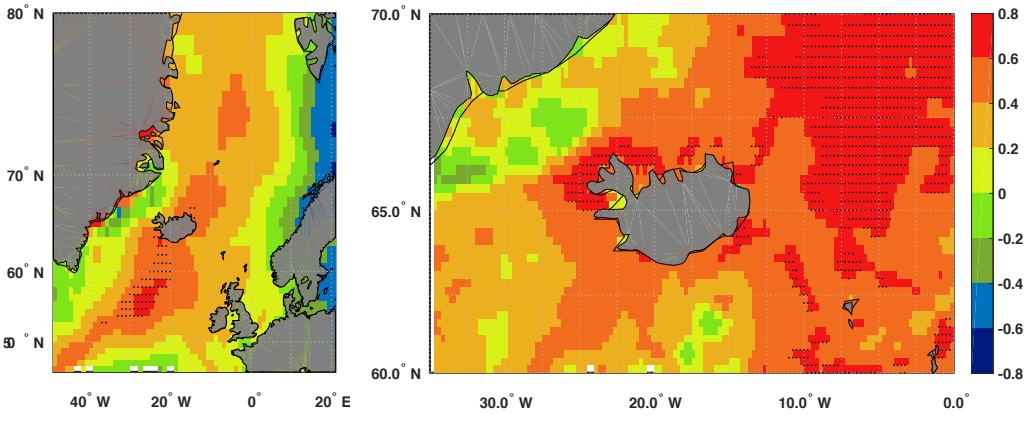

960 FIG. 8. Correlations between annual DS inflow and wind from south (left) and SSH (right). Dots indicate
961 significant correlations.

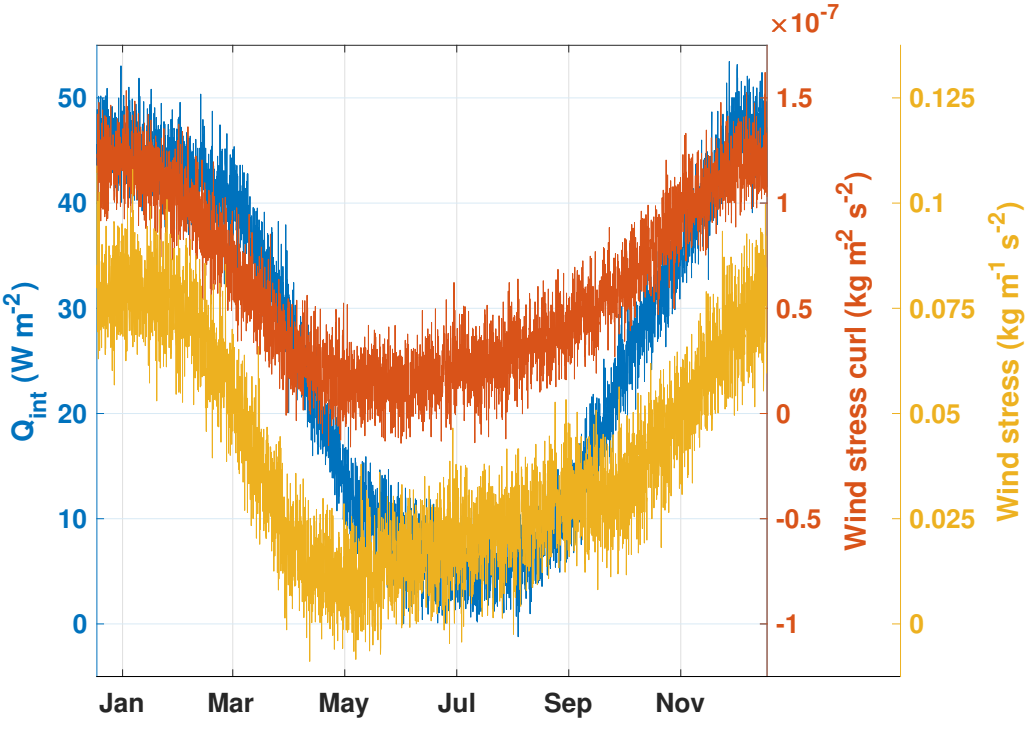

962 FIG. 9. Applied forcing for the two-layer model. Seasonal cycles of atmospheric heat flux for the interior,
963 Q_{int}, wind stress curl and wind stress.

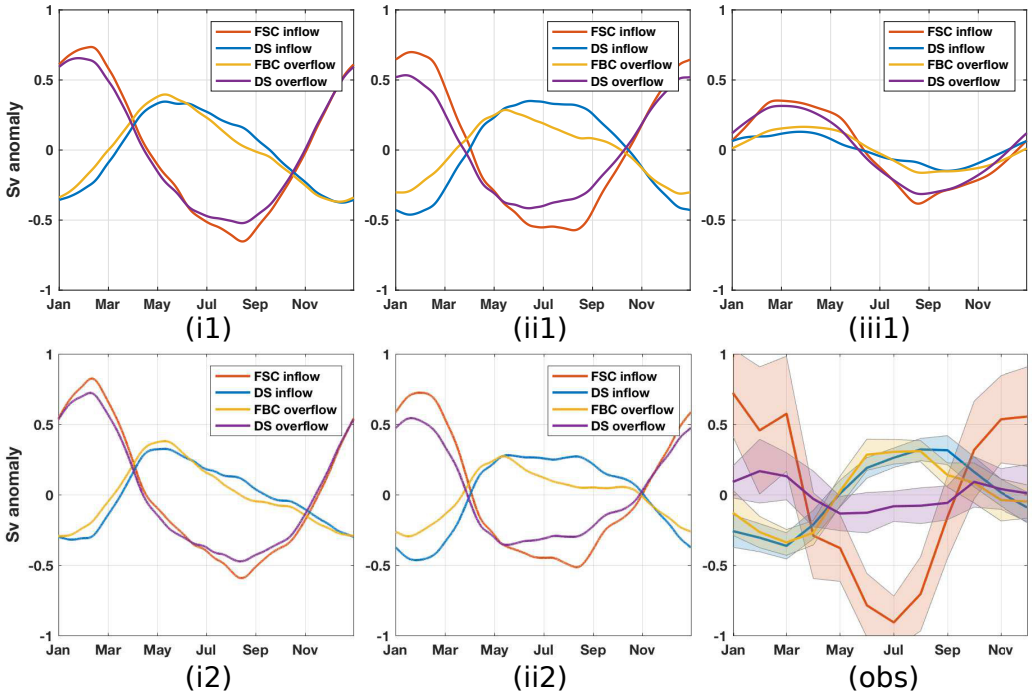

964 FIG. 10. Seasonal cycles of the in- and outflow of the two-layer model. Resulting seasonal cycles when the
965 model is forced with: (i) seasonally varying atmospheric heat flux and wind (left); (ii) seasonally varying wind
966 and constant atmospheric heat flux (middle); and, (iii) seasonally varying atmospheric heat flux and constant
967 wind (right). In the first row wind forcing is through wind stress curl using (1), while in the second row wind
968 forcing is through wind stress using (2). The two cases applying constant wind forcing, (iii1) and (iii2), give
969 equal results. The bottom right plot (obs) instead shows the average seasonal cycles from Figure 2. Exchanges
970 are given same names and sign convention as in Figure 2. All curves from the two-layer model are low-pass
971 filtered with a 1month Hanning filter.

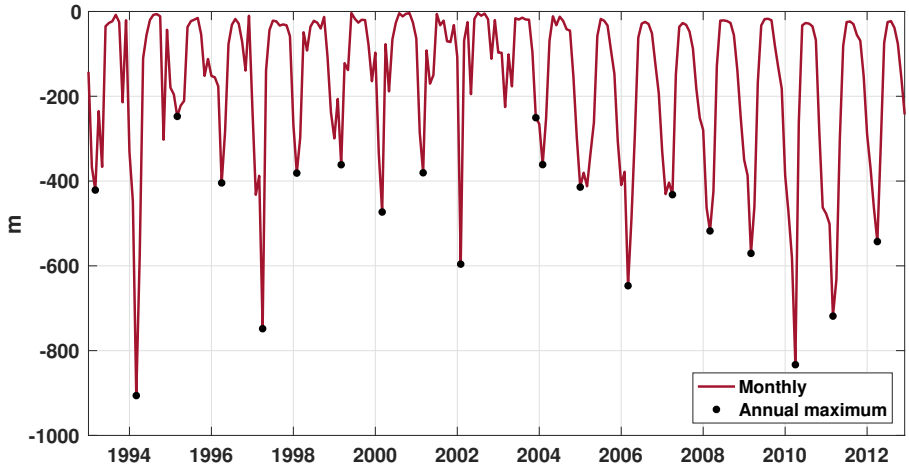

FIG. 11. Norwegian Sea mixed layer depth. Monthly (red) and annual maximum (black dots) regionally averaged MLD over 66°-71°N, 10°W-5°E.

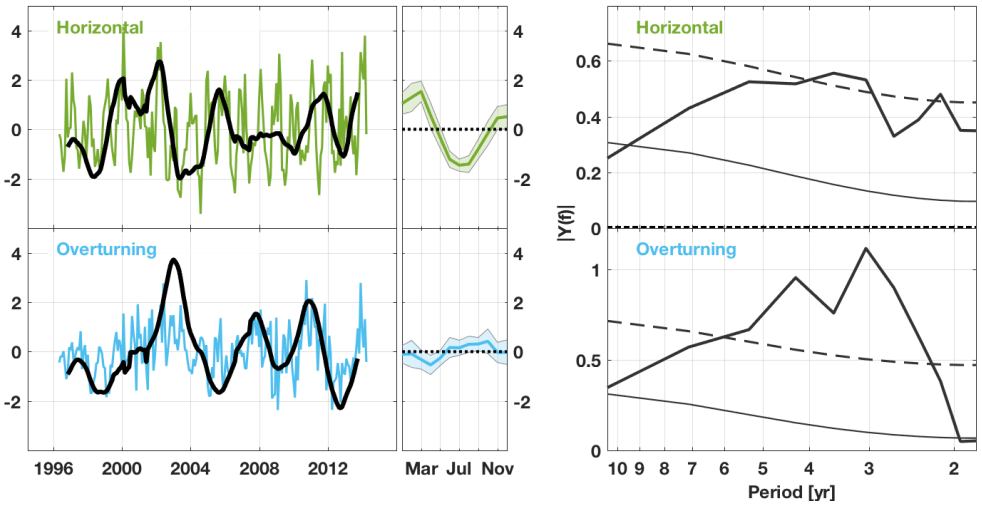

974 FIG. 12. Horizontal and overturning circulation in the Nordic Seas. Left: PCs of monthly EOFs representing
975 horizontal (top) and overturning (bottom) in colors, with corresponding PCs of annual data as black overlay.
976 The y-axis reflects standardized anomalies. Middle: Average seasonal cycles of the monthly PCs with 95%
977 errorbars. Right: Power spectra of the monthly PCs (with seasonal cycle removed) together with red noise (thin
978 line) and 95% confidence level (thin dashed line).

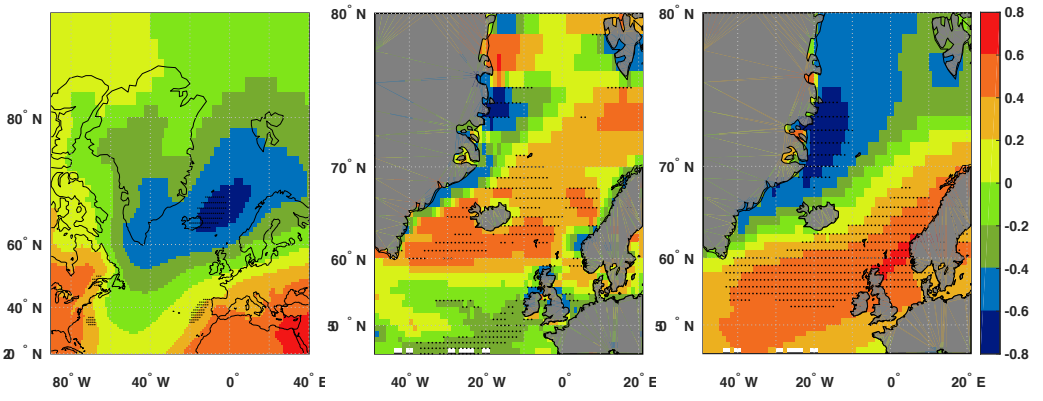

FIG. 13. Atmospheric forcing of the seasonal horizontal circulation. Correlation maps between the monthly horizontal circulation (PC1) and gridded SLP (left), wind stress curl (middle) and southwesterly wind stress (right). Dots indicate significant correlations.

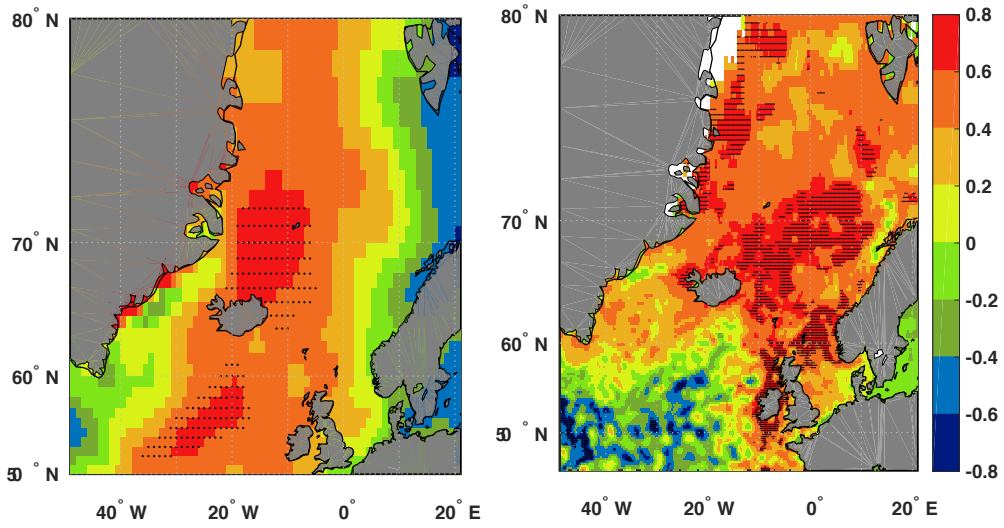

FIG. 14. Atmospheric forcing of the annual overturning circulation. Correlation maps between the annual overturning circulation (PC1) and gridded southern winds (left) and SSH (right). Dots indicate significant correlations.